THE JOURNAL OF PHYSICAL CHEMISTRY C

pubs.acs.org/JPCC Article

Impact of Spin-Exchange Interaction on Charge Transfer in Dual-Polymer Photovoltaic Composites

Victor I. Krinichnyi,* Evgeniya I. Yudanova, Nikolay N. Denisov, Aleksei A. Konkin, Uwe Ritter, Bernhard Wessling, Alexander L. Konkin, and Victor R. Bogatyrenko

Cite This: J. Phys. Chem. C 2020, 124, 10852−10869

ABSTRACT: Magnetic resonance, relaxation, and dynamic parameters of spin-charge carriers photoinitiated in dual-polymer composites formed by narrow-band-gap poly[(9,9-dioctylfluorenyl-2,7-diyl)-alt-(bithiophene)] (F8T2), poly[2,7-(9,9-dioctylfluorene)-alt-4,7-bis(thiophen-2-yl)benzo-2,1,3-thiadiazole] (PFO-DBT), and poly[*N*-9′-heptadecanyl-2,7-carbazole-alt-5,5-(4′,7′-di-2-thienyl-2′,1′,3′-benzothiadiazole)] (PCDTBT) copolymers modified with [6,6]-phenyl-C_{61}-butanoic acid methyl ester ($PC_{61}BM$) as a photovoltaic spin subsystem and polyaniline salt doped with *para*-toluenesulfonic acid (PANI:TSA) as a guest spin subsystem were comparatively studied by the direct light-induced electron paramagnetic resonance (LEPR) spectroscopy in a wide photon energy and temperature range. Irradiation of dual-polymer composites by the photons leads to the formation in its photovoltaic subsystem of polarons and methanofullerene radical anions whose concentration and dynamics are determined by the density and energy of the initiating light photons. A part of such polarons first filled high-energetic spin traps formed in the matrix due to its disordering. A crucial role of exchange interaction between different spin ensembles in the charge excitation, relaxation, and transport in multispin narrow-band-gap composites was demonstrated. These processes were interpreted within the framework of hopping of polarons along copolymer chains of photovoltaic subsystems and their exchange interaction with neighboring spin ensembles. Such an interaction was shown to facilitate the transfer of charges and inhibit their recombination in multispin dual-polymer composites. The distribution of spin density over polymer chains in the dual-polymer composites with the $\pi-\pi$ stacked architecture was analyzed in the framework of the density functional theory (DFT). It confirmed the transfer of electron spin density between neighboring polymer chains that made formation more likely of radical pairs in triplet state than in singlet one and inhibited their fast geminate recombination. Spin interactions eliminate the selectivity of these systems to the photon energy, extend the range of optical photons they absorb, and, therefore, increase their efficiency to converse the light energy. Handling electronic properties via intra- and intersubsystem spin interactions in such multispin composites allows one to create on their base more efficient and functional electronic and spintronic elements.

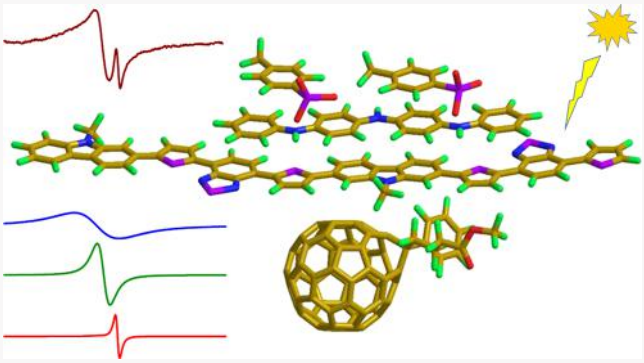

1. INTRODUCTION

Recent years have been characterized by an increasing interest in the synthesis and study of organic polymers and composites due to the great potential of their use as functional materials for creating components of molecular electronics[1−3] and spintronics.[4] Elemental charges in such compounds are carried by quasi-particles, polarons, which are characterized by their effective mass, intrachain fast diffusion, and uncompensated spin $S = 1/2$. These features lead to a variety of specific processes that can be carried out in such low-dimensional systems. Molecular devices normally consist of fullerene derivatives embedded into a functional polymer matrix, which act as acceptors (electron transporter, n-type material) and donors (hole transporter, p-type material) of electrons. Beyond the transformation of photoinduced excitons into pairs of two opposite charges and their separation into respective bulk heterojunctions (BHJs), positive carriers are transported to electrodes by polaron quasi-one-dimensional (Q1D) diffusion in the polymer phase and by free electron hopping between fullerene domains. Such carriers can be considered noninteracting when the thermal energy exceeds their interaction integral. In the opposite case, when the carriers come nearer than the inverted Coulombic interaction

Received: March 16, 2020
Revised: April 16, 2020
Published: April 22, 2020

https://dx.doi.org/10.1021/acs.jpcc.0c02317
J. Phys. Chem. C 2020, 124, 10852−10869

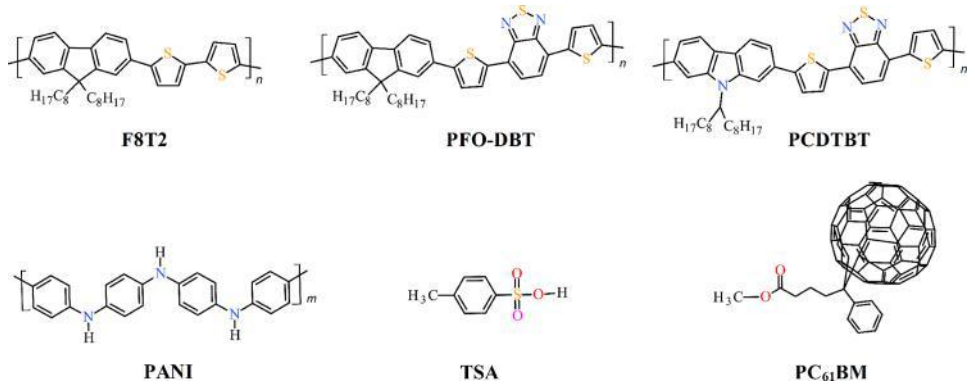

Figure 1. Schematic structures of the poly[(9,9-dioctylfluorenyl-2.7-diyl)-*co*-(bithiophene)] (F8T2), poly[2,7-(9,9-dioctylfluorene)-alt-4,7-bis(thiophen-2-yl)benzo-2,1,3-thiadiazole] (PFO-DBT), poly[*N*-9′-heptadecanyl-2,7-carbazole-alt-5,5-(4′,7′-di-2-thienyl-2′,1′,3′-benzothiadiazole)] (PCDTBT), polyaniline (PANI), *para*-toluenesulfonic acid (TSA), and [6,6]-phenyl-C_{61}-butanoic acid methyl ester ($PC_{61}BM$) used for preparation of the dual-polymer composites.

potential, their wave functions overlap and exchange interactions become non-negligible. This should affect the electronic properties of the respective composite and thus the efficiency of its conversion of the light energy. Spin interactions also accelerate the recombination of these charge carriers, leading to a balance of the excited and recombined spin pairs. Because both the charge carriers have an exchangeable spin-flip, the recombination process becomes dependent on their dynamics, number, polarization, and mutual separation.[5] Thus, the efficiency and functionality of the above systems are governed mainly by spin-assisted separation, coupling, and recombination of free charge carriers formed in BHJ.

Among polymer-based molecular devices, polymer:fullerene photovoltaic composites have been more widely investigated and used.[6−8] The narrow-band-gap copolymer poly[*N*-9″-heptadecanyl-2,7-carbazole-alt-5,5-(4′,7′-di-2-thienyl-2′,1′,3′-benzothiadiazole)] (PCDTBT; see Figure 1) appeared[9,10] to be one of the most efficient matrixes for use in organic electronics and photonics. This can be attributed mainly to the ultrafast charge separation in the BHJ formed by PCDTBT and [6,6]-phenyl-C_{71}-butyric acid methyl ester ($PC_{71}BM$) before localization of the primary excitation to form a bound exciton[11] and also its "column-like" bilayer ordered copolymer matrix, where a pair of backbones is positioned "side-by-side" with the alkyl side chains pointing outward.[12] Besides, higher π-overlapping in such quasi-two-dimensional (Q2D) copolymers hinders their torsional twisting and, therefore, lowers their band gap.[13] Such a morphology increases the lamella crystallinity of narrow-band-gap copolymer composites, accelerates the mobility of charge carriers, elongates their diffusion length, and thus inhibits their recombination in their BHJ.[14] The small number of excitons initially formed in such a matrix recombines fast for nanoseconds and thus does not contribute to an effective photocurrent through BHJ, whereas the main part of excitons dissociates into free charge carriers on a longer time scale, which contributes to the photocurrent and then nongeminate recombination. However, Yonezawa et al. have supposed[15] that in the copolymer BHJ formed by poly[(9,9-dioctylfluorenyl-2,7-diyl)-alt-(bithiophene)] (F8T2) and $PC_{71}BM$ molecules, positively charged polarons are created mainly by direct photogeneration and not by conversion from the interfacial charge-transfer states. Besides, one would not expect the recombination of each charge carrier with the first/nearest oppositely charged one. The experimental data obtained from the study of polymer composites are usually interpreted in terms of the processes occurring in the backbone of single polymer chains with solitary spin ensembles. However, the coupling of spins of charge carriers moving along adjacent polymer chains, as well as those captured by corresponding spin traps, significantly affects all of the properties of the carriers and a whole composite and should therefore be taken into consideration. Thus, these processes themselves are not trivial phenomena, whose microscopic details still remain unknown.

Different methods can be used for the study of organic photovoltaic systems, e.g., femtosecond time-resolved optically[15] and absorption-detected[16] magnetic resonance methods. These methods, however, are indirect and can mainly determine a net number of centers formed from an initial exciton and recombined in the respective BHJ. Because both charge carriers possess spins playing a crucial role in the properties of organic devices, the processes carried out in such systems can be studied by various continuous wave (cw) and pulse magnetic resonance methods. However, the latter often provide ambiguous results concerning spin-coupling, relaxation, and dynamics in some conjugated polymers[17−19] and in polymer:fullerene composites.[20,21] This is the reason why direct cw electron paramagnetic resonance (cw EPR) spectroscopy is widely used for a more detailed investigation of spin-assisted processes in various organic polymer systems at different frequencies of electron precession.[18,19,22−24] The multifrequency cw EPR method was used to analyze the impact of exchange interaction between polarons stabilized in polyaniline salt highly doped with *para*-toluenesulfonic acid (PANI:TSA) with guest air oxygen biradicals.[25−28] PANI-TSA was analyzed[29] to be a material built from relatively short helically formed chains that assemble within globular particles of size about 10 nm. Paramagnetic centers stabilized in the PANI bulk during doping with TSA were found to be more accessible for interaction with inside/guest radicals than with other polyaniline salts. Light-induced cw EPR (LEPR) spectroscopy was also used for the study of charge photoexcitation, separation, transfer, and recombination in various polymer:fullerene composites.[30−34] It was found that the *g*-factors of both charge carriers photoinitiated in such systems are close to the *g*-factor of the free electron, $g_e = 2.00232$. This causes partial or complete overlapping of their contributions to the total cw LEPR spectra registered at relative low precession

https://dx.doi.org/10.1021/acs.jpcc.0c02317
J. Phys. Chem. C 2020, 124, 10852−10869

frequency of their spin ensembles. The lower this frequency, the more the spectral overlapping. Therefore, for a more accurate analysis of the influence of all possible factors on magnetic resonance parameters (paramagnetic susceptibility, line width, *g*-factor) of all spin ensembles, one has to deconvolute the effective spectra obtained at commonly used[34,35] and high-frequency[23,36,37] cw LEPR wavebands. Deconvolution of effective cw LEPR spectra of a multispin system should be able to determine the main magnetic resonance parameters separately for all mobile and captured spin-charge carriers and analyze them upon variation of experimental conditions. Indeed, such a procedure allows one to estimate the composition, spatial distribution, and local concentration of spin-charge carriers excited in different organic photovoltaic composites,[34] including narrow-band-gap mono-copolymer composites formed by F8T2, poly[2,7-(9,9-dioctylfluorene)-alt-4,7-bis(thiophen-2-yl)benzo-2,1,3-thiadiazole] (PFO-DBT), and PCDTBT copolymers with $PC_{61}BM$ electron acceptors,[38−42] BHJ of various poly(3-alkylthiophenes):C_{60} embedded into the conducting poly(2,5-dioctyloxy-phenylene vinylene) matrix (P3AT:C_{60}/OOPPV)[43] as well as dual-polymer composites formed by $PC_{61}BM$-modified poly(3-dodecylthiophene) and PANI:TSA (PANI:TSA/P3DDT:$PC_{61}BM$).[27,28] Paramagnetic susceptibility of spin-charge carriers photoinitiated in the latter dual-polymer composites was determined from their cw LEPR spectra to follow antiferromagnetic or ferromagnetic behavior depending on the value of spin-coupling. It was shown that the number, composition, and distribution of paramagnetic centers excited in the mono- and bipolymer photovoltaic systems are determined by their structure, morphology, as well as by the density and energy of the initiating light photons. The data obtained were interpreted assuming the presence in photovoltaic systems of high-energy spin traps that capture the first charge carriers until they are filled. Thus, immobilized carriers take part in the process of charge transfer, however, indirectly. A part of such carriers can be released upon interaction with the light photons and lattice phonons of a certain energy. For example, the concentration of polarons captured in the F8T2T:$PC_{61}BM$ copolymer composite appeared to demonstrate dependence on the photon energy with explicit extremes around 1.8 and 2.7 eV, whereas such dependence of the methanofullerene radical anions showed a weaker dependence with the characteristic energy lying near 1.9 eV. At the same time, the concentration of both charge carriers in the PFO-DBT:$PC_{61}BM$ and PCDTBT:$PC_{61}BM$ systems is characterized by a dependence on the photon energy with explicit extremes around 1.8 and 2.8 eV. So, the number, spatial distribution, and energy depth of such traps significantly determine the functional and electronic properties of these and analogous systems. The main magnetic resonance parameters as well as electron relaxation and dynamics of spin-charge carriers stabilized or/and photoinitiated in these BHJ were interpreted in the framework of the model of exchange-coupled spin pairs differently distributed in parental polymer subsystems. This leads to the higher overlapping of wave functions of spin-charge carriers, increases the energy barrier that they overcome by crossing the respective BHJ, and accelerates electron relaxation of all spin-packets formed in such systems. Analysis of spin density distribution (SDD) on polymer chains within the density functional theory (DFT) can provide unique information on the degree of delocalization and interaction of polarons stabilized and photoinitiated in this system.

Herein, we report the first results of a detailed comparative cw LEPR study of spin-assisted photoexcitation, relaxation, dynamics, and recombination of charge carriers in the framework of their exchange interaction in the dual-polymer narrow-band-gap PANI:TSA/F8T2:$PC_{61}BM$, PANI:TSA/PFO-DBT:$PC_{61}BM$, and PANI:TSA/PCDTBT:$PC_{61}BM$ nanocomposites. The data obtained by cw LEPR spectroscopy at a wide temperature and photon energy range in combination with spectral simulations and DFT computation allowed us to determine the correlations of the main parameters of photoinitiated spin-charge carriers with the structure, composition, and lattice phonons of these compounds. The data obtained are compared with those determined by some other methods.

2. EXPERIMENTAL SECTION

2.1. Ingredients Used in Experiments. In the work, poly[(9,9-dioctylfluorenyl-2,7-diyl)-alt-(bithiophene)] (F8T2) with an optical absorption maximum lying at 3.40 eV (365 nm) and band-gap energy ΔE_g = 2.40 eV (ref 44) (manufactured by American Dye Source, Inc.), poly[2,7-(9,9-dioctylfluorene)-alt-4,7-bis(thiophen-2-yl)benzo-2,1,3-thiadiazole] (PFO-DBT) with an optical absorption maximum lying at 2.37 eV (523 nm) and ΔE_g = 1.87 eV (ref 45) (distributed by Sigma-Aldrich, The Netherlands), and poly[*N*-9′-heptadecanyl-2,7-carbazole-alt-5,5-(4′,7′-di-2-thienyl-2′,1′,3′-benzothiadiazole)] (PCDTBT) with an optical absorption maximum lying at 576 nm (2.15 eV) and ΔE_g = 1.90 eV (refs 46, 47) (distributed by Sigma-Aldrich, the Netherlands) were used as electron donors of photovoltaic subsystems, and [6,6]-phenyl-C_{61}-butanoic acid methyl ester ($PC_{61}BM$) with ΔE_g = 2.48 eV (ref 48) (distributed by Solenne BV, the Netherlands) was used as an electron acceptor of photovoltaic subsystems. Polyaniline salt (PANI) doped with *para*-toluenesulfonic acid (PANI:$TSA_{0.5}$) (manufactured by Ormecon, Germany) (ref 29) was used as the guest spin ensemble. The chemical structures of these components are shown schematically in Figure 1.

2.2. Preparation of the Samples. To prepare copolymer:methanofullerene composites with an optimal concentration ratio 1:4,[46] first 1.4 mg of each copolymer and 5.6 mg of $PC_{61}BM$ were solved in 1 mL of dichlorobenzene. These solutions were treated in the ultrasonic cleaner DADI DA-968 (50 W) for 15 min, followed by warming at T = 333 K for 5 h. In a second step, for the preparation of PANI:TSA/PFO-DBT:$PC_{61}BM$ and PANI:TSA/PCDTBT:$PC_{61}BM$ dual-polymer composites, a dichlorobenzene dispersion (10^{-2} M) of PANI:$TSA_{0.5}$ was pretreated by an ultrasonic source for 10 min and then added to each of the above-mentioned copolymer:methanofullerene solutions to reach an equal content of these ingredients in the final dispersion. To prepare the PANI:TSA/F8T2:$PC_{61}BM$ dual-polymer composite, 5 μL of the PANI:TSA dichlorobenzene dispersion (10^{-2} M) was pretreated by an ultrasonic source for 10 min and then added into 40 μL of the F8T2:$PC_{61}BM$ solution. The concentrations of the PANI:TSA and F8T2:$PC_{61}BM$ ingredients in the latter were found to be 2.2×10^{-3} and 2.6×10^{-3} M, respectively. Thus, 5 μL of the prepared liquid samples were each cast 6−8 times on both sides of a separate ceramic plate with subsequent drying in air until they became double-sided films, both having size ca. 4 × 8 mm^2 and thickness ca. 0.1 mm. As a result of such a procedure, each sample contained in sum 0.1 mg of a

https://dx.doi.org/10.1021/acs.jpcc.0c02317
J. Phys. Chem. C 2020, 124, 10852−10869

copolymer, 0.4 mg of $PC_{61}BM$, and 0.02 mg of PANI:TSA. All dual-polymer composites are shown schematically in Figure 1.

2.3. NIR−Vis−UV Absorption Spectra of Copolymer Composites. Optical absorption spectra of the dual-polymer composites were obtained using the spectrophotometer Specord-250 plus (Analytik Jena) scanning in the range 1.13−6.53 eV (1100−190 nm) at T = 298 K. They are shown in Figure S1 in comparison with the spectra obtained for the respective copolymer photovoltaic composites.[42] The compositions and positions of the spectral components were determined accurately using the differentiation of experimental absorption spectra.

2.4. Photoinitiation of Spin-Charge Carriers. The samples were illuminated directly in the MW cavity of the EPR spectrometer through a quartz cylindrical light guide by 5−10 W Luxeon LED monochromatic sources with the photon energy $h\nu_{ph}$/wavelength λ_{ph}/luminous emittance I_l of 1.32 eV/940 nm/750 lx, 1.46 eV/850 nm/870 lx, 1.61 eV/770 nm/1160 lx, 1.88 eV/660 nm/1950 lx, 1.97 eV/630 nm/1110 lx, 2.10 eV/590 nm/450 lx, 2.34 eV/530 nm/960 lx, 2.48 eV/500 nm/1500 lx, 2.64 eV/470 nm/2450 lx, 2.95 eV/420 nm/1520 lx, and 3.14 eV/395 nm/630 lx, as well as achromatic, white sources with correlated color temperatures (CCTs) of T_c = 15 000, 5500, and 3300 K and luminous emittance values I_l of 3020, 4000, and 2480 lx, respectively. The I_l values of the sources were determined using the IMO-2N broadband bolometric light emission power meter and the LX-1010BS digital luxmeter and were used for further normalization of the number of spins photoinitiated in the composites under study.

2.5. LEPR Spectra Measurements and Processing. cw EPR measurements were performed using the X-band (3 cm, 9.7 GHz) PS-100.X spectrometer with a maximum microwave power of 150 mW and 100 kHz phase detection. Dark and photoinduced LEPR spectra of the dual-polymer:methanofullerene nanocomposites were obtained at 77 K by being inserted into a quartz Dewar filled with liquid nitrogen and placed into the EPR spectrometer cavity. For EPR measurements at higher temperatures (T = 90−320 K), the samples were situated in a quartz flow Dewar cell and centered in a stream of dry nitrogen, whose temperature was stabilized by a BRT SKB IOC controller, equipped with a platinum temperature sensor pt100. The signal-to-noise ratio of signals was improved by their accumulation during multiple scanning of the EPR spectra. The processing of the spectra was performed using EPR-Win and OriginLab software. Spectral contribution and concentration of different spin ensembles were determined by decomposing effective EPR spectra registered far from their MW saturation and in combination with the "light on−light off" procedure described earlier.[34,49,50] Landé g-factors of spin-charge carriers were determined using the N,N-diphenyl-N'-picrylhydrazyl (DPPH) standard with g = 2.0036 ± 0.0002.[51] The accuracy of estimating the intensity I, the g-factor of the line, and the distance between its positive and negative spectral peaks ΔB_{pp} was determined to be 5%, ± 2×10^{-4}, and ± 2×10^{-3} mT, respectively. The times of spin−lattice T_1 and spin−spin T_2 relaxation of spin ensembles were determined using the steady-state MW saturation method,[52] adapted for the study of spin pairs photoinitiated in organic polymer:fullerene nanocomposites.[53] The calculation of hyperfine coupling parameters has been performed using the DFT/B3LYP/G level in ORCA with 6-311G** and partly EPR-III basis sets as has been described in refs 36, 37. The simulation of experimental EPR spectra was performed using the EasySpin and OriginLab programs.

3. RESULTS AND DISCUSSION

3.1. NIR−Vis−UV Absorption Spectra of Copolymer Composites. Figure S1 shows the NIR−vis−UV spectra of the PANI:TSA/F8T2:$PC_{61}BM$, PANI:TSA/PFO-DBT:$PC_{61}BM$, and PANI:TSA/PCDTBT:$PC_{61}BM$ dual-polymer composites. For the comparison, optical spectra obtained[42] for respective copolymer photovoltaic composites are also shown in Figure S1. The spectrum of PANI:TSA/F8T2:$PC_{61}BM$ is characterized by bands 339, 268, 218 nm (3.66, 4.63, 5.69 eV), 338, 268, 219 nm (3.67, 4.63, 5.66 eV), and 339, 269, 221 nm (3.66, 4.61, 5.61 eV), respectively, whose positions are close to those obtained for F8T2:$PC_{61}BM$,[42] differing by a slight growth in optical density at the high-energy region due to the overlapping signals of both polymers. The system PANI:TSA/PFO-DBT:$PC_{61}BM$ demonstrates a characteristic set of absorption bands at 608 and 571 nm (2.04 and 2.17 eV) inherent to the benzatriazole moiety and lines at 415 and 397 nm (2.99 and 3.12 eV) attributed to the fluorine subunits. The composite PANI:TSA/PCDTBT:$PC_{61}BM$ is characterized by the bands registered at 610 and 569 nm (2.03 and 2.18 eV) arising due to the benzothiadiazole molecular fragment as well as at 416 and 397 nm (2.98 and 3.12 eV) arising due to the carbazole subunit. Structurally, the latter two absorption spectra also correspond to those earlier obtained for the PFO-DBT:$PC_{61}BM$ and PCDTBT:$PC_{61}BM$ composites.[42] The only difference is that the presence of the PANI:TSA subsystem increases the intensity of the UV−vis absorption band at near 290 nm, typical of a $\pi-\pi^*$ transition.[54,55] Thus, polyaniline salt, while dispersed in these composites, leads to a slight increase in the density of optical spectra while maintaining their structures. This effect becomes more noticeable at the transition from the F8T2 and PCDTBT subsystems to the PFO-DBT one.

3.2. DFT Evaluation of the Morphology and Radical Spin Density Overdistribution in the PCDTBT/PANI $\pi-\pi$ Stacking Model Complex. The main part of the ingredients of organic solar cells is not bonded covalently, and hence an intermolecular charge transfer occurs in terms of the Arrhenius activation electron hopping through an appropriate energy barrier whose height depends dramatically on the morphology interface. As for the electron spin-exchange process in the samples under study, the most significant interest seems to be in the evaluation of transfer of spin density between the chains in the BHJ of copolymers and PANI. Such an approach is based on the spin flip−flop mechanism,[56] according to which the geminate recombination of radical pairs (RPs) in the singlet state is suppressed by resonant exchange coupling between radicals with spin S = 1/2 and electron acceptors with formation of RP in the triplet state. Because the RP triplet species should have a longer lifetime due to their "spin-forbidden" state, this indeed could reduce the geminate recombination rate. The above approach was used supposing the resonant exchange coupling between spins of polarons stabilized in PANI and photoinitiated in copolymer backbones and taking into account the fact that the highest occupied molecular orbital (HOMO) levels of copolymers and doped PANI are close to each other, i.e., −5.2 eV for doped PANI salt and −5.4, −5.5, and −5.75 eV for F8T2, PCDTBT, and PFO-TBT, respectively. The density functional theory (DFT) evaluation was carried out with the exemplary PCDTBT-

https://dx.doi.org/10.1021/acs.jpcc.0c02317
J. Phys. Chem. C 2020, 124, 10852−10869

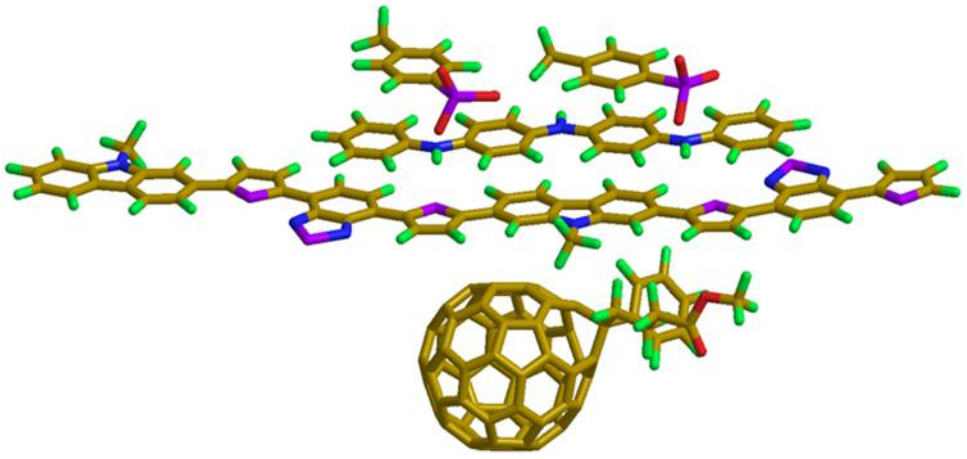

Figure 2. Hypothetical model structure of an exemplary PANI:TSA/PCDTBT:$PC_{61}BM$ composite with the discussed $\pi-\pi$ stack morphology of polymers whose C, H, N, O, and S atoms are displayed in dark yellow, green, blue, red, and violet, respectively.

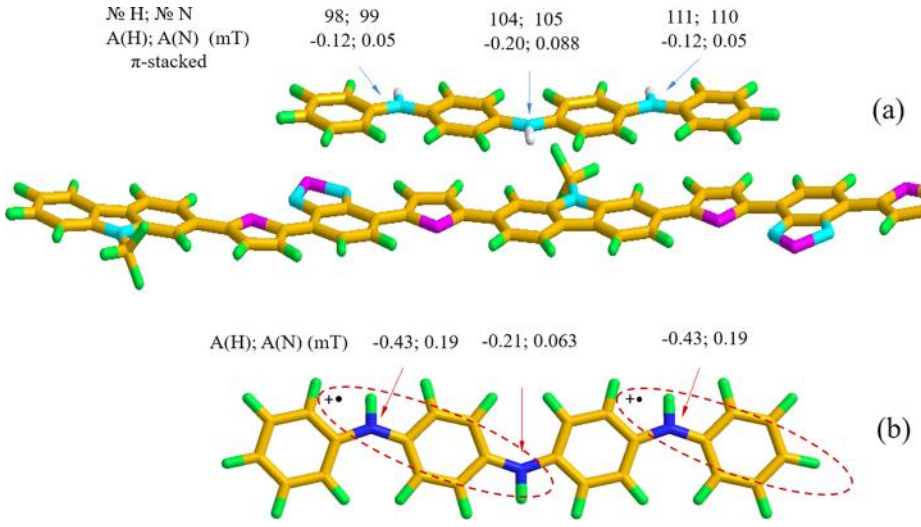

Figure 3. (a) $\pi-\pi$ Stacking PCDTBT/PANI architecture used in the DFT calculation of evaluation of the hyperfine coupling. (b) Spin/charge localization in a separated PANI chain.

based system. One could suggest the realization of the $\pi-\pi$ stacks as the most suitable architecture of these copolymers, which suggests the principle of $\pi-\pi$ interaction between identical aromatic groups; however, such an interaction is realized between their different groups. The $\pi-\pi$ stacking morphology in PANI is already widely known;[57] however, the existence of an analogous architecture in the copolymers under study has not yet been described in the literature. The hypothetic model structure of the PANI:TSA/PCDTBT:$PC_{61}BM$ dual composite with the supposed $\pi-\pi$ stacking polymer morphology is exhibited in Figure 2, and the Cartesian coordinate data of 4ANI:2TSA/2CDTBT:$PC_{61}BM$ and 4ANI/2CDTBT are listed in Tables S1 and S2 of the Supporting Information. Such an architecture seems to be preferable regarding the PANI and $PC_{61}BM$ positions relative to PCDTBT when it realized free donor/acceptor contact in the interface area from one side and effective connection due to $\pi-\pi$ overlapping of polymer and copolymer stacks from the other side. For the optimization of such a $\pi-\pi$ stacking block structure, the standard force field (FF) calculation methods, e.g., MM2 and MMFF94, have been used, resulting in the minimum of steric energy corresponding to the above 3D molecular architecture of two polymers with $\pi-\pi$ stacking interactions. Note that the distance between the stacked planes of the most aromatic molecules of the PANI:TSA/PCDTBT system was determined to be about $d_1 \approx d_2 \approx 3.4-3.5$ Å (see Figures 2 and S3), which correlates with the data obtained experimentally by X-ray diffraction (XRD) and other methods for analogic structures.[58−61] During the DFT calculation, the available processing power sometimes becomes limited, thus necessitating great simplification of the working model. This is demonstrated as an example in Figure 3, where the $(-CH_2)_n$-CH_3 side chains of the copolymer are reduced essentially down to $-CH_3$. Such a simplification weakly changes the spin density distribution (SDD) along polymer chains of the same length; however, it drastically shortens the computation time. The evaluation of appropriate hfc parameters for ^1H atoms on the polymer side chains >N-$(CH_2)_3$-CH_3 and >N-CH_3 of the CDTBT unit is exhibited in **SI−IIc**, and it confirms the possibility of the above tail substitution in the computation process. However, the experimental realities should be taken into account. First, it should be noted that the delocalization of polarons photoinduced on the chains of PCDTBT and analogous copolymers is usually longer at least by one

https://dx.doi.org/10.1021/acs.jpcc.0c02317
J. Phys. Chem. C 2020, 124, 10852−10869

monomer, which decreases the SDD magnitudes. While the processing time decreases substantially, this circumstance should also be taken into consideration.

The second circumstance concerning the π-stacking area is how many charges/spins of the PANI may overlap directly with π-orbitals in the π-stacking side fragment. Because PANI has the maximum doping level, for evaluation, only two charges/spins were included in the input sets shown in Figure 3b. DFT hfc parameter calculation of: (a) ANI dimer (4ANI, charge Ch = +2, spin S = 1, multiplicity M = 2S + 1 = 3), (b) CDTBT dimer (CDTBTd, Ch = +1, S = 1/2, M = 2), and (c) 4ANI/CDTBTd block (Ch = 3, S = 3/2, M = 4) structures exhibited in Figure 3a were carried out using the DFT/B3LYP/G level in ORCA.[62] Figure 4 shows the constants A_H

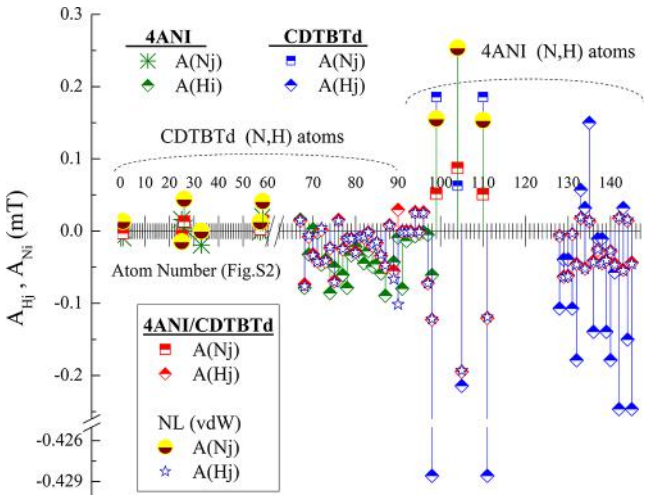

Figure 4. DFT isotropic hfc parameters A(Nj) and A(Hi) are calculated for CDTBTd, 4ANI, and 4ANI/CDTBTd model structures. DFT sets are in the text. The assignation of an appropriate "magnetic" atom numbers is displayed in Figure S2 in Supporting Information (SI).

and A_N calculated for the system under study. Their values, $A_H \approx 0.43$ mT and $A_N \approx 0.2$ mT, lie near $A_H \approx A_N \approx 0.6$ mT, reported in the literature tentatively and near those obtained for the aniline oligomer by the ^{1}H ENDOR method in the range 1.6−5.3 MHz,[63] that correlates by magnitudes with maximum ones for ^{1}H in regions (nos. 128−146) shown in Figure 4. It can be seen from the figure that the SDD on some ^{1}H CDTBTd atoms and on the same atoms in the ANI/CDTBTd system calculated in terms of the considered models differs by several times in atom number region nos. 67−97. The same tendency is evidently observed for H and N atoms of the ANI dimer situated within the range nos. 98−146 (Figure 4). The computed SDD data demonstrate the possibility of essential SD overdistribution within both copolymer molecules with $\pi-\pi$ interactions. Some examples of this topic based on PDI family composites including $\pi-\pi$ stacking architectures are introduced in ref 36 and references therein.

As for the ANI/CDTBTd, i.e., in our case of a completely ionic complex, van der Waals (vdW) contribution became essential and should be checked in the single point energy and SDD/hfc calculation. For this, the nonlocal van der Waals density functional VV10 (DFT-NL)[64,65] was used with the B3LYP NL/def2-TZVP/C/vdwgrid2 set, and the result (yellow-brown cycles in Figure 4) demonstrates tripling correction for A(Nj) parameters in the 4ANI/CDTBTd complex relatively values, calculated without vdW contribution (red-white squares in Figure 4). This results in the effective EPR line width of the ANI/CDTBTd complex computed with the vdW functional being close to the PANI line width obtained without the vdW one, due to the close contribution from hfc to the line-broadening, and in this case, ENDOR application could be useful. Unfortunately, our experimental opportunities are limited toward this goal. However, taking into account the "resonant" close location of their higher molecular orbitals (HOMOs) noted above, this may evidence the absence of principal obstacles for the relatively free electron transfer between copolymer systems.[56] The analysis of the data obtained from DFT computing allows us to emphasize at least two points as being important for the processing of experimental EPR results. First is the spin exchange in systems, whose EPR spectra are broadened due to hyperfine coupling (hfc). The other is the hfc contribution to the line width ΔB of the spectra of the dual-polymer composite analyzed. The analysis of the ^{1}H DFT data obtained for PCDTBT allowed us to conclude that, e.g., its seven ^{1}H [A(Hj) ≈ 0.075 mT] and six ^{1}H [A(Hj) ≈ 0.055 mT] with individual δB = 0.4 mT give the same spectrum as the line without hfc contribution and δB = 0.45 mT. This means that the value of line width of PCDTBT determined experimentally may deviate due to hfc; however, the respective contribution does not exceed 12%. On the other hand, an analogous analysis of the data presented in Figure 5a evidences that the model spectrum of PANI with δB

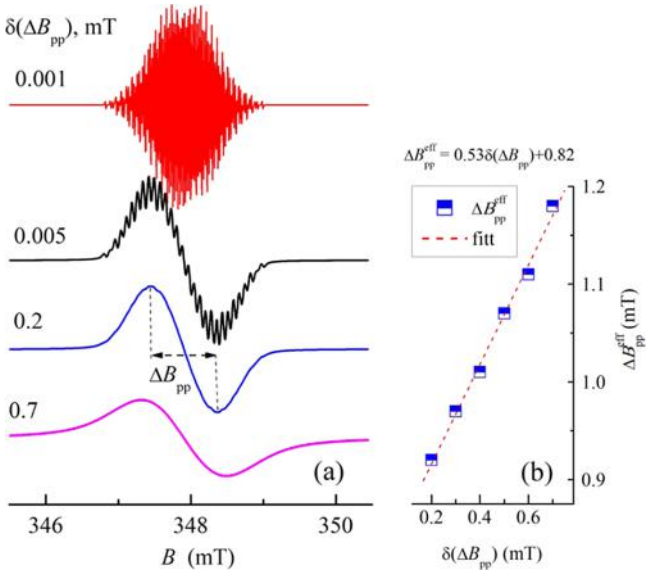

Figure 5. ANI EPR spectra, constructed using A_N = 0.2, 0.07 mT; A_H = 0.45, 2(0.225), 0.175, 3(0.175), 0.1 mT; and individual line width $\delta(\Delta B_{pp})$ = 0.001, 0.005, 0.2, 0.3, 0.4, 0.5, 0.6, 0.7 mT (spectra with 0.3, 0.4, 0.5, and 0.6 are not included in the figure). In the inset are shown the experimental $\Delta B_{pp} = F(\delta B_{pp})$ functional dependence and its fitting by a linear function approach.

= 1.2 mT without hfc contribution can be coincident with its DFT computed line A_N = 0.2, 0.07 mT; A_H = 0.45, 2(0.225), 0.175, 3(0.175), 0.1 mT; and δB_{pp} = 0.2 mT. This allowed us to evaluate inhomogeneous line-broadening of the EPR spectrum by directly modeling a spectrum with an unresolved hfc structure. In Figure 5a are shown the exemplary ANI EPR spectra, constructed using A_N = 0.2, 0.07 mT; A_H = 0.45, 2(0.225), 0.175, 3(0.175), 0.1 mT; and individual line width

https://dx.doi.org/10.1021/acs.jpcc.0c02317
J. Phys. Chem. C 2020, 124, 10852−10869

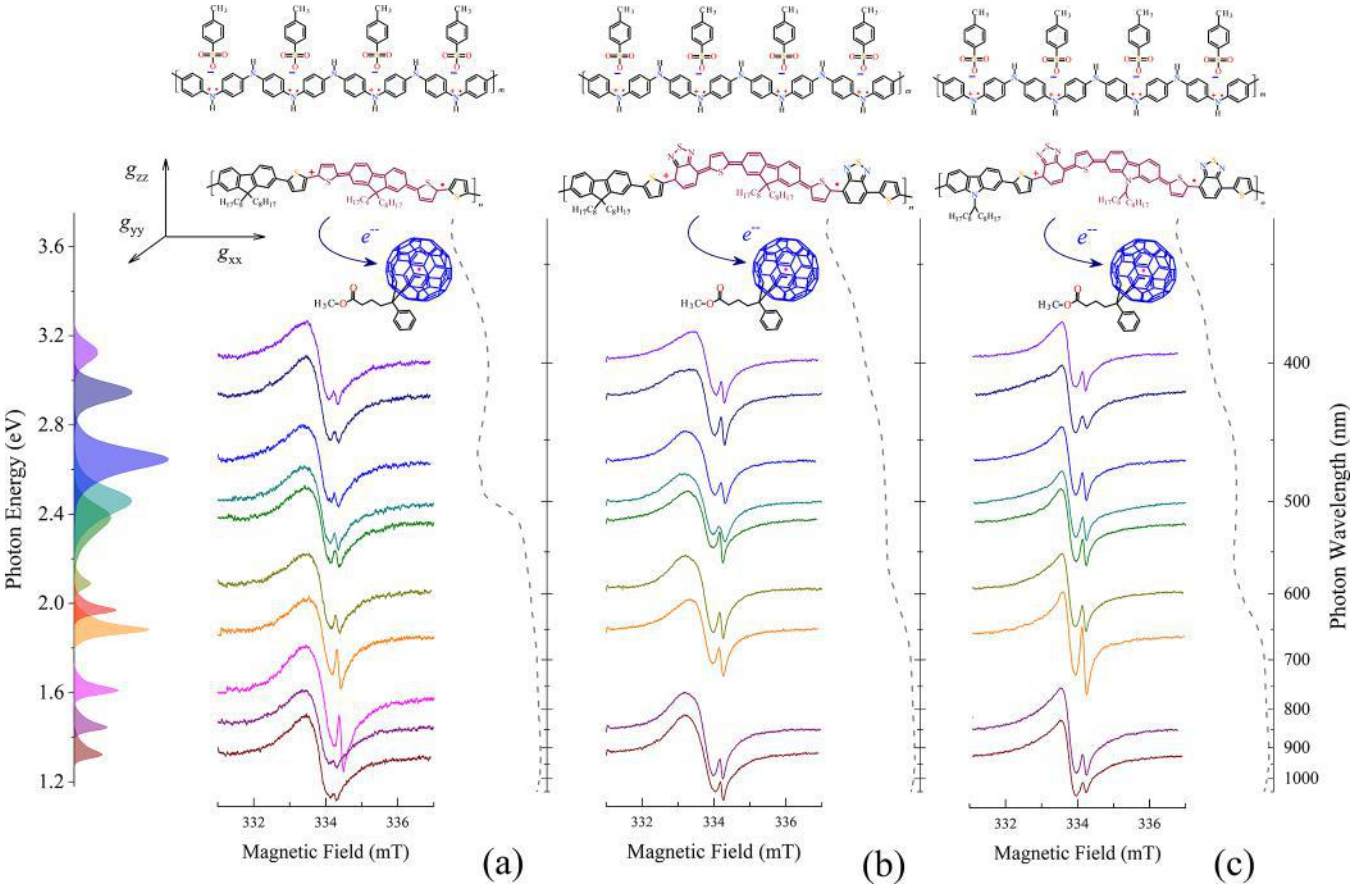

Figure 6. Some X-band (9.5 GHz, 334 mT) LEPR spectra of charge carriers that are background initiated in the PANI:TSA/F8T2:$PC_{61}BM$ (a), PANI:TSA/PFO-DBT:$PC_{61}BM$ (b), and PANI:TSA/PCDTBT:$PC_{61}BM$ (c) BHJ at T = 77 K by monochromatic light sources with different photon energies. Respective room-temperature NIR−vis−UV absorption spectra of these composites are located on the right and are shown by dashed lines. Translucent filled lines located on the left indicate irradiation spectra of the light sources normalized to their luminous emittance I_l. At the top, the structures of BHJ formed in the dual-polymer nanocomposites are shown schematically. The transfer of an elementary negative charge from the copolymer chain to the methanofullerene molecule accompanied by the formation on the former of positively charged polaron $P^{+\bullet}$ (hole) with spin $S = 1/2$ is shown as well. The spin of such quasi-particles normally occupies a larger ($n \geq 3$) number of copolymer monomers than shown in the figure. The orientation of the principal axes of the polaron's g-tensor is also given.

$\delta(\Delta B_{pp})$ = 0.001, 0.005, 0.2, 0.3, 0.4, 0.5, 0.6, 0.7 mT. Analysis of the data showed a linear functional dependence of the experimental line width ΔB_{pp} on its actual individual value $\delta(\Delta B_{pp})$ (Figure 5b). From the slope of the function $\Delta B_{pp} = F[\delta(\Delta B_{pp})]$, a simple relation of these values was obtained as follows: $\delta(\Delta B_{pp}) = (\Delta B_{pp} - 0.82)/0.53$ or $\delta(\Delta B_{pp}) = 0.6\Delta B_{pp}$ for a brief estimation within the range of our experimental values around 1.1−1.2 mT.

3.3. Spin Composition and Magnetic Resonance Parameters. Figure 6 shows exemplary X-band LEPR spectra of the PANI:TSA/F8T2:$PC_{61}BM$, PANI:TSA/PFO-DBT:$PC_{61}BM$, and PANI:TSA/PCDTBT:$PC_{61}BM$ BHJ backgrounds irradiated by monochromatic sources with various photon energies $h\nu_{ph}$ at T = 77 K. Figure 7 exhibits the analogous spectra of the samples illuminated by white light with different correlated color temperatures (CCTs) T_c. Earlier, it was shown[40−42] that at this waveband, the F8T2:$PC_{61}BM$, PFO-DBT:$PC_{61}BM$, and PCDTBT:$PC_{61}BM$ BHJ demonstrate doublet LEPR spectra of organic paramagnetic centers formed as a result of dissociation of photoinitiated excitons. As in the case of other similar photovoltaic composites,[34] the low-field component of these spectra was attributed to polarons, formed on the copolymer chains, whereas the high-field spectral line refers to methanofullerene radical anions situated between these chains. These paramagnetic centers are characterized by isotropic Landé g-factors lying near $g_{iso} = 2.002_1$−2.002_4 and $g_{iso} = 1.999_{89}$.[42] Such parameters obtained for the polarons stabilized in the initial PANI:TSA powder were determined at the D-waveband (2 mm, 140 GHz) EPR to be $g_{iso} = 2.0028_0$.[25] Thus, their spectra should be expected to overlap those of polarons photoinitiated in the copolymer:methanofullerene subsystem, as it is realized in the case of the PANI:TSA/P3DDT:$PC_{61}BM$ dual-polymer composite.[27] This means that the broader low-field LEPR spectral line of the samples under study shown in Figures 6 and 7 can be attributed to polarons stabilized and photoinitiated in the PANI and copolymer matrices, respectively, whereas their narrower right line appears due to methanofullerene radical anions also photoinitiated in the latter. The low-field line contains the contributions of mobile polarons with an isotropic g-factor, as well as polarons captured by spin traps formed in the composite matrix due to its disordering. Polarons immobilized in conjugated polymers and their photovoltaic composites are characterized by a weakly anisotropic g-factor[34,35,66] and frequency-dependent line width due to its g-strain. This means that the shape of the sum spectrum of all polarons should depend on the number of such traps. The effect of g-strain is very small at the X-band EPR

https://dx.doi.org/10.1021/acs.jpcc.0c02317
J. Phys. Chem. C 2020, 124, 10852−10869

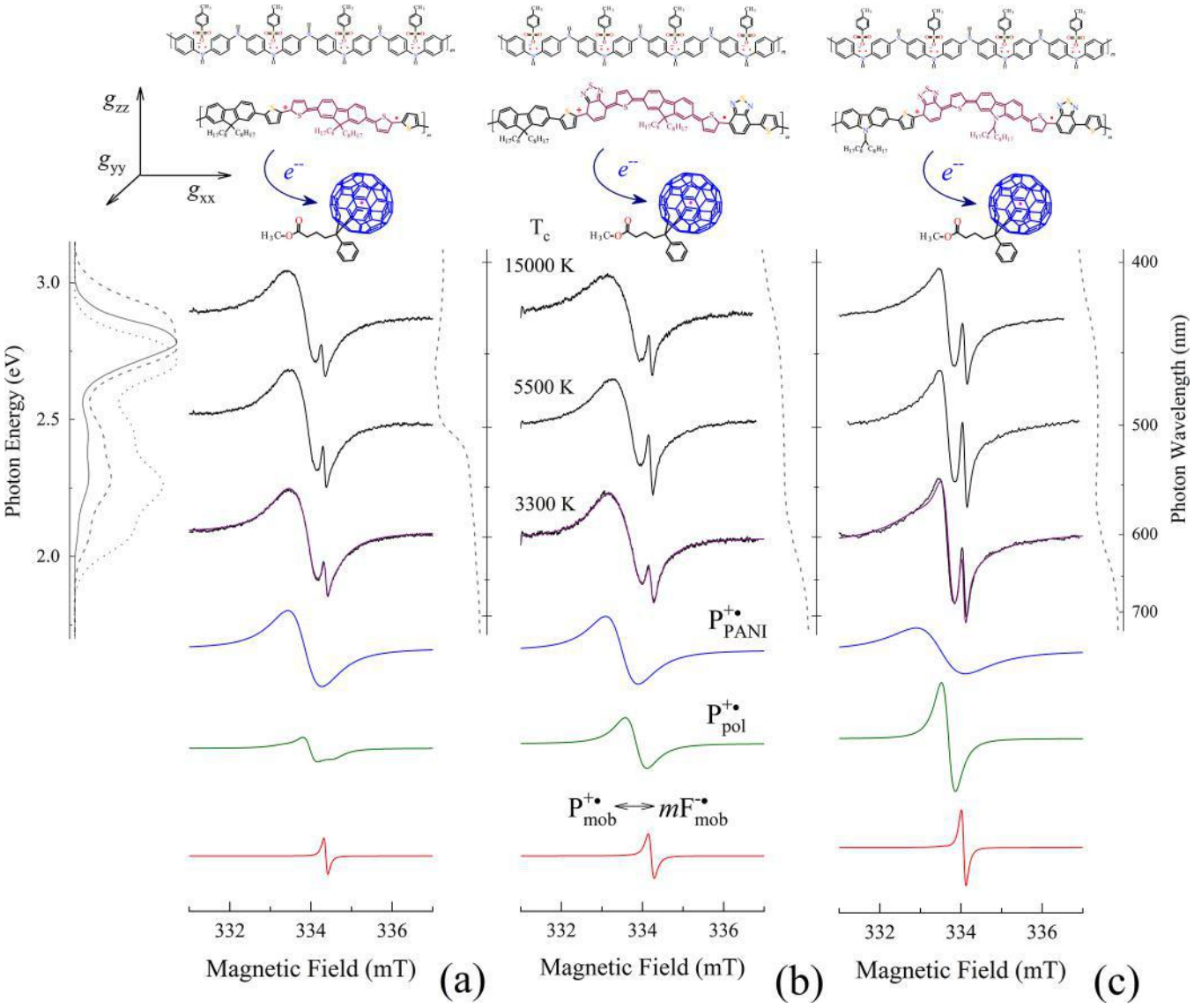

Figure 7. X-band (9.5 GHz, 334 mT) LEPR spectra of charge carriers that are background initiated in the PANI:TSA/F8T2:$PC_{61}BM$ (a), PANI:TSA/PFO-DBT:$PC_{61}BM$ (b), and PANI:TSA/PCDTBT:$PC_{61}BM$ (c) BHJ at T = 77 K by achromatic, white light with CCT of T_c = 15 000, 5500, and 3300 K. Solid, dashed, and dotted lines located on the left indicate the irradiation spectra of the white light sources with T_c = 15 000, 5500, and 3300 K, respectively, normalized to their blue spectral line lying near 450 nm. Dashed lines located on the right indicate respective room-temperature NIR−vis−UV absorption spectra of these composites. Lorentzian LEPR spectra best fitting the effective experimental LEPR spectra with their contributions caused by polarons stabilized in the PANI:TSA, $P^{+\bullet}_{PANI}$, polarons immobilized in a copolymer matrix, $P^{+\bullet}_{loc}$, as well as highly mobilized radical pairs, $P^{+\bullet}_{mob} \leftrightarrow mF^{-\bullet}_{mob}$, illuminated by white light with CCT of T_c = 3300 K using the parameters presented in Table 1 are shown at the bottom of the figure. At the top are schematically shown the structures of BHJ formed in respective dual-polymer nanocomposites. The transfer of an elementary negative charge from the copolymer chain to the methanofullerene molecule accompanied by the formation on the former of polaron $P^{+\bullet}$ (hole) with an elementary positive charge and spin S = 1/2 is shown as well. The spin of such a quasi-particle normally occupies a larger ($n \geq 3$) number of copolymer monomers than shown in the figure. The orientation of the principal axes of the polaron's g-tensor is also given.

used; however, it was taken into account when calculating the spectra. Besides, polarons forming in adjacent polymer chains, starting with some critical concentration, can, in principle, collapse into interchain mobile diamagnetic $P^{+\bullet}_{mob} \leftrightarrow P^{+\bullet}_{mob}$ or intrachain localized paramagnetic $P^{-\bullet}_{loc} \leftrightarrow P^{+\bullet}_{loc}$ bipolarons with equal g-factors.[67,68] The transition polaron ↔ bipolaron can change the experimental LEPR spectra as well. To separate the contributions of different charge carriers into the sum LEPR spectra and to analyze their changes at different experimental conditions, such spectra should be deconvoluted according to the procedure described earlier.[35,42] In Figure 7, the dashed lines represent the effective LEPR spectra and their spectral contributions due to polarons $P^{+\bullet}_{PANI}$ and $P^{+\bullet}$ stabilized in the PANI and photoinitiated in copolymer matrices, respectively, as well as mobile pairs of polarons and methanofullerene radical anions $P^{+\bullet}_{mob} \leftrightarrow mF^{-\bullet}_{mob}$ photoinitiated in the copolymer backbone of the samples by white light with T_c = 3300 K. This allowed one to obtain separately the main magnetic resonance, electron relaxation, and dynamic parameters for all spins at a wide variation of experimental conditions. It can be seen from Figures 6 and 7 that the relative concentration of charge carriers stabilized and photoinitiated in the samples studied

https://dx.doi.org/10.1021/acs.jpcc.0c02317
J. Phys. Chem. C 2020, 124, 10852−10869

Table 1. Isotropic *g*-Factors of Polarons, Initiated in the PANI and Copolymer Backbones, g_{iso}^{PANI} and g_{iso}^{P}, Respectively, Their Methanofullerene Radical Anions' Peak-to-Peak Line Widths, ΔB_{pp}^{PANI}, ΔB_{pp}^{P}, and ΔB_{pp}^{mF}, Concentration Ratio of Mobile Polarons and Methanofullerene Radical Anions to that of Localized Polarons, $n_{mob}^{p,mF}/n_{loc}^{P}$, Spin−Lattice and Spin−Spin Relaxation Times of Polarons, T_1^{PANI} and T_2^{PANI}, T_1^{P} and T_2^{P}, and Methanofullerene, T_1^{mF} and T_2^{mF}, Respectively, Coefficients of Polaron Diffusion Along D_{1D}^{PANI} and D_{1D}^{P} and Between D_{3D}^{PANI} and D_{3D}^{P} Polymer Chains, and Methanofullerene Hopping Libration Near its Main Molecular Axis, D_{lb}^{mF}, Determined Under Steady-State Illumination of the Composites Under Study by Achromatic White Light with Different Correlated Color Temperatures, T_c at T = 77 K

	PANI:TSA/F8T2:$PC_{61}BM$			PANI:TSA/PFO-DBT:$PC_{61}BM$			PANI:TSA/PCDTBT:$PC_{61}BM$		
				T_c, K					
parameter	15 000	5500	3300	15 000	5500	3300	15 000	5500	3300
g_{iso}^{PANI}	2.002_{89}	2.002_{87}	2.002_{92}	2.003_{87}	2.003_{41}	2.003_{59}	2.002_{59}	2.003_{14}	2.00328
g_{iso}^{P}	2.002_{36}	2.002_{38}	2.002_{36}	2.002_{21}	2.002_{51}	2.002_{22}	2.002_{19}	2.002_{50}	2.00_{201}
ΔB_{pp}^{PANI},[a] mT	0.830	0.817	0.838	0.921	0.897	0.803	1.095	1.120	1.004
ΔB_{pp}^{P}, mT	0.331	0.345	0.340	0.578	0.449	0.467	0.319	0.307	0.303
ΔB_{pp}^{mF}, mT	0.096	0.099	0.097	0.105	0.117	0.132	0.121	0.119	0.117
n_{mob}^{mF}/n_{loc}^{P}	0.023	0.022	0.021	0.002	0.047	0.011	0.161	0.107	0.167
T_1^{PANI}, s	3.61×10^{-7}	3.93×10^{-7}	8.50×10^{-7}	3.22×10^{-7}	3.64×10^{-7}	9.96×10^{-7}	5.53×10^{-7}	2.03×10^{-7}	3.86×10^{-7}
T_2^{PANI}, s	7.90×10^{-9}	8.02×10^{-9}	7.82×10^{-9}	7.12×10^{-9}	7.31×10^{-9}	8.17×10^{-9}	5.99×10^{-9}	5.86×10^{-9}	6.53×10^{-9}
T_1^{P}, s	9.68×10^{-7}	4.24×10^{-7}	3.21×10^{-7}	1.10×10^{-6}	2.86×10^{-7}	2.37×10^{-7}	1.99×10^{-7}	1.57×10^{-7}	2.20×10^{-7}
T_2^{P}, s	1.98×10^{-8}	1.90×10^{-8}	1.93×10^{-8}	1.13×10^{-8}	1.46×10^{-8}	1.40×10^{-8}	2.06×10^{-8}	2.14×10^{-8}	2.16×10^{-8}
T_1^{mF}, s	1.48×10^{-6}	9.28×10^{-7}	1.07×10^{-6}	4.41×10^{-7}	8.08×10^{-7}	3.33×10^{-7}	5.55×10^{-7}	3.86×10^{-7}	3.85×10^{-7}
T_2^{mF}, s	6.85×10^{-8}	6.61×10^{-8}	6.78×10^{-8}	6.25×10^{-8}	2.98×10^{-8}	4.67×10^{-8}	5.42×10^{-8}	5.51×10^{-8}	5.62×10^{-8}
D_{1D}^{PANI}, rad/s	1.13×10^{13}	1.30×10^{13}	5.82×10^{13}	1.12×10^{12}	2.54×10^{12}	$7.04 \times 1\ 0^{12}$	2.33×10^{12}	3.79×10^{11}	1.08×10^{12}
D_{3D}^{PANI}, rad/s	4.71×10^{6}	4.09×10^{6}	8.17×10^{5}	4.83×10^{6}	3.96×10^{6}	6.47×10^{5}	1.14×10^{6}	8.56×10^{6}	2.81×10^{6}
D_{1D}^{P}, rad/s	3.12×10^{11}	7.62×10^{10}	3.05×10^{10}	6.98×10^{11}	5.91×10^{10}	2.89×10^{10}	2.36×10^{10}	1.81×10^{10}	2.65×10^{10}
D_{3D}^{P}, rad/s	4.11×10^{6}	2.07×10^{7}	3.81×10^{7}	1.03×10^{6}	2.70×10^{7}	3.68×10^{7}	1.21×10^{8}	2.25×10^{8}	1.10×10^{8}
D_{lb}^{mF}, rad/s	2.10×10^{11}	2.69×10^{11}	3.93×10^{11}	5.94×10^{12}	1.16×10^{11}	1.87×10^{12}	7.68×10^{10}	1.15×10^{11}	1.31×10^{11}

[a]Note: A main part of the PANI line width is due to hfc (see Section 3.2).

depends not only on the structure of dual-polymer composites but also on the energy and spectral characteristics of the light sources.

In the sections discussed next, we consider the main magnetic resonance parameters of spin-charge carriers stabilized and photoinitiated in the samples under study upon their steady-state illumination by monochromatic light sources, and these parameters obtained at their excitation by white light with different CCT T_c are summarized in Table 1.

3.4. Spin Susceptibility. The LEPR spectra shown in Figures 6 and 7 are the sum spectra of polarons stabilized in the PANI:TSA salt and the net spectra of spin-charge carriers photoinitiated and recombined in the respective copolymer:-methanofullerene BHJ. It has been shown previously[39−42] that the number and composition of paramagnetic centers photo-initiated in the latter are determined by their structure, morphology, and temperature as well as by the density and energy of the initiating light photons. Similar peculiarities should be expected also for the dual-polymer composites under study. The analysis of these properties becomes simpler on analyzing the ratio of the concentrations of mobile charge carriers to the localized ones. Indeed, with a higher concentration ratio of mobile methanofullerene radical anions (and polarons) to that of localized polarons, $n_{mob}^{mF}/n_{loc}^{P} \equiv n_{mob}^{P}/n_{loc}^{P}$, the charges separated in the BHJ should be transferred to electrodes easier and faster, therefore leading to better efficiency of energy conversion for the respective photovoltaic system.

Figure 8 depicts the relative concentration of polarons $P_{PANI}^{+\bullet}$ stabilized in the PANI:TSA subsystem and the ratios $n_{mob}^{p,mF}/n_{loc}^{P}$ determined for the mobile and captured polarons $P_{loc}^{+\bullet}$, as well as of methanofullerene radical anions $mF_{mob}^{-\bullet}$ photoinitiated in the F8T2:$PC_{61}BM$, PFO-DBT:$PC_{61}BM$, and PCDTBT:$PC_{61}BM$ copolymer subsystems as a function of the temperature and energy of initiating photons $h\nu_{ph}$. The main feature of the data presented in Figure 8a is the extreme performance of the $n_{mob}^{p,mF}/n_{loc}^{P}$ ratios obtained for the F8T2:$PC_{61}BM$, PFO-DBT:$PC_{61}BM$, and PCDTBT:$PC_{61}BM$ subsystems with characteristic extremes situated near $h\nu_{ph}$ = 1.8, 1.8, and 2.3 eV, respectively. It should be noted that analogous dependences were obtained for these photovoltaic composites with peaks lying near $h\nu_{ph}$ = 1.9, 2.0, and 1.7 eV, respectively.[39−41] Such a peculiarity was explained to be a result of the specific morphology and band structure of these systems with inhomogeneously distributed high-energetic spin traps and different energy levels occupied by spins in their band gap. Besides, this can occur if some immobilized polarons are realized from deep spin traps under the action of photons of a corresponding energy. The shift of the extreme points may be due to changes in the number and energy depth of spin traps, as well as the number of captured polarons released from them in the samples under study. This is especially evident when mixing the PANI:TSA subsystem with the PCDTBT:$PC_{61}BM$ one when the respective dual-polymer composite becomes more sensitive to photons at the energy increase by ca. 0.6 eV. This effect can be used, e.g., for creation of light band-converters and filters. It is seen from the figure that the PANI:TSA subsystem being combined with the F8T2:$PC_{61}BM$ BHJ also demonstrates analogous dependence of polaron concentration on the photon energy. This can be as a result of a stronger exchange interaction between different spin ensembles in the PANI:TSA/F8T2:$PC_{61}BM$ dual-polymer composite. The results obtained evidence that the integration of polymer and copolymer subsystems with interacting spin ensembles changes structural and electronic properties of the resulting system.

https://dx.doi.org/10.1021/acs.jpcc.0c02317
J. Phys. Chem. C 2020, 124, 10852−10869

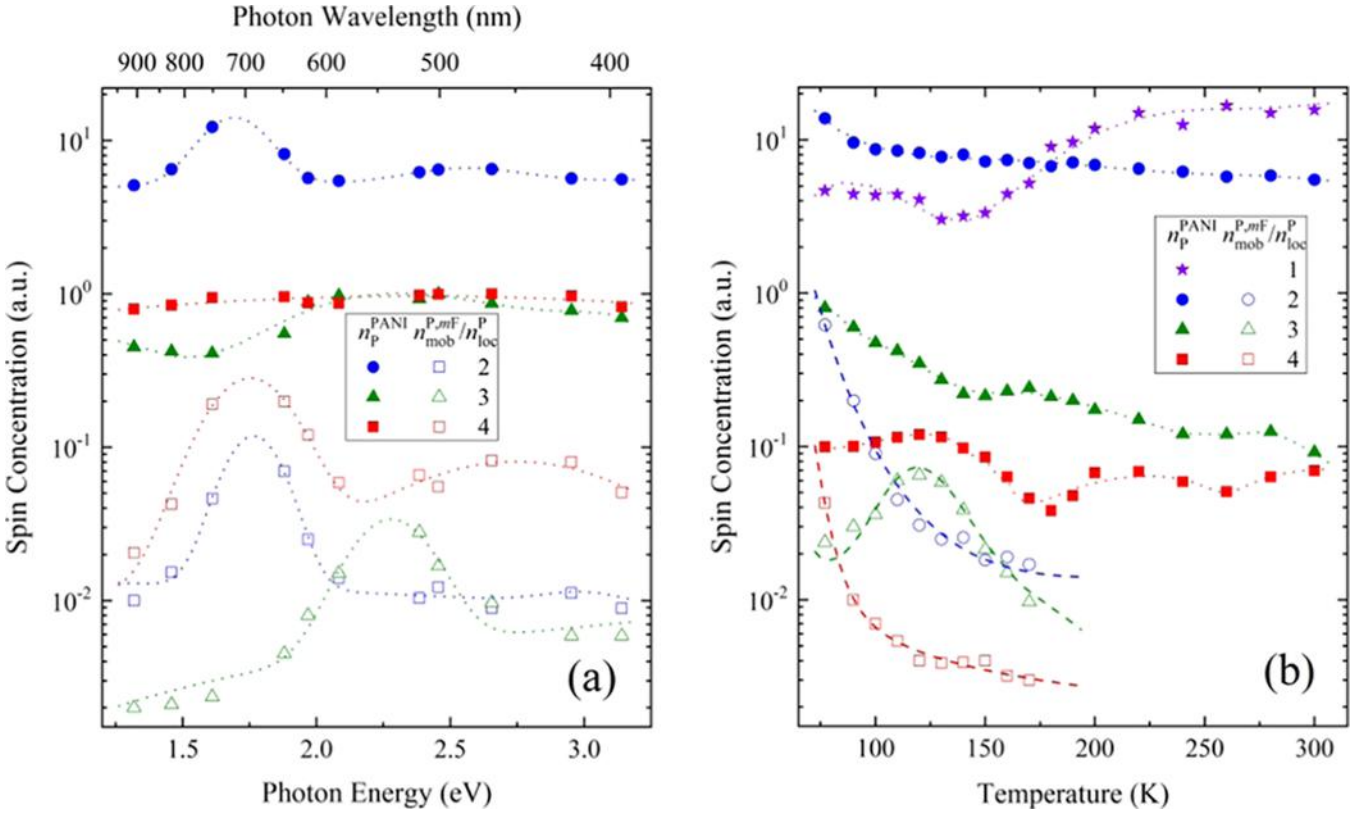

Figure 8. Spin concentration of polarons $P^{+\bullet}_{PANI}$ stabilized in the PANI:TSA subsystem, n_P^{PANI}, (1) and concentration ratio of mobile polarons $P^{+\bullet}_{mob}$ and methanofullerene radical anions $mF^{-\bullet}_{mob}$ to that of localized polarons $P^{+\bullet}_{loc}$, $n^{P,mF}_{mob}/n^{P}_{loc}$, photoinitiated in the F8T2:PC_{61}BM (2), PFO-DBT:PC_{61}BM, (3) and PCDTBT:PC_{61}BM (4) subsystems as a function of photon energy $h\nu_{ph}$ at T = 77 K (a) and temperature at CCT T_c = 5500 K (b). The values obtained were normalized to the luminous emittance of the light sources I_l. The dashed lines connecting in (b) the experimental open circle, triangle, and square points were calculated from eq 1 with ΔE_{ij} = 0.034 eV and E_a = 0.019 eV, ΔE_{ij} = 0.072 eV and E_a = 0.037 eV, and ΔE_{ij} = 0.023 eV and E_a = 0.012 eV, respectively, and J_{ex} = 0.093 eV. The other lines are drawn arbitrarily only for illustration to guide the eye.

Figure 8b also shows the dependences of the concentration parameters n_P^{PANI} and $n^{P,mF}_{mob}/n^{P}_{loc}$ of the samples under study on the temperature. The data presented show that the number of polarons stabilized in the initial PANI:TSA system slightly increases with temperature. Such a change correlates with an analogous dependence of the spectral line width of these centers (see below) and may have originated due to the coupling of spin-charge carriers stabilized in the polymer backbone. However, when this subsystem is combined with a photovoltaic one, the $n^{P,mF}_{mob}/n^{P}_{loc}$ ratio of the latter begins to decrease with temperature increase, just as it does in other organic solids with spin additives. This may be due to the dilution of polyaniline chains in dual-polymer composites. The most significant temperature change is registered for the $n^{P,mF}_{mob}/n^{P}_{loc}$ value of these systems. This parameter of samples PANI:TSA/F8T2:PC_{61}BM and PANI:TSA/PCDTBT:PC_{61}BM decreases sharply with temperature increase up to 170 K due to acceleration of the recombination of both mobile charge carriers. On the other hand, this parameter of the PANI:TSA/PFO-DBT:PC_{61}BM sample demonstrates an extreme temperature dependence with a characteristic point lying near T = 120 K. Analogous dependence was obtained for spin susceptibility of some P3AT:C_{60}/OOPPV dual-polymer composites demonstrating antiferromagnetic ↔ ferromagnetic balance.[43] It should be emphasized that somewhat faster processes with analogous peculiarities were registered in our previous study[42] of copolymer composites, which have been used in the present work as photovoltaic subsystems. It was shown that the $n^{P,mF}_{mob}/n^{P}_{loc}$ ratio of the F8T2:PC_{61}BM and n^{P}_{loc} parameters of the PFO-DBT:PC_{61}BM composites demonstrates extreme temperature dependences with characteristic points lying around T = 170 and 120 K, respectively, which was explained by an exchange interaction of mobile charge carriers with the other spin ensembles in these systems. Such an effect was shown to be realized in various multispin polymer systems[34] due to the implementation of regimes of strong and weak spin-coupling at lower and higher temperatures, respectively.[25,27,69] It can be assumed that in this case, heating of the sample can shift the balance between these regimes and, thereby, release some additional charge carriers captured in high-energy spin traps. Undoubtedly, such processes should also be realized in multipolymer composites with a larger number of spin ensembles.

According to the Miller−Abrahams tunneling model,[70] a polaron diffusing between initial i and final j sites of a single polymer chain spends the difference of its energies ΔE_{ij}. In a real polymer system, its interaction with the other spins should also be taken into account.[71,72] The amplitude of such an interaction is determined mainly by the spin density on each polymer unit and the rate of spin intrachain diffusion with the expenditure of energy ΔE_{ij}. Generally, the relation for the effective paramagnetic susceptibility of polarons with spin S = 1/2 can be written as[28,69,73]

$$\chi(\Delta E_{ij}, E_a) = \chi_0 \frac{2(1+\alpha^2)}{\alpha^2} \exp\left(\frac{\Delta E_{ij}}{k_B T}\right) \quad (1)$$

https://dx.doi.org/10.1021/acs.jpcc.0c02317
J. Phys. Chem. C 2020, 124, 10852−10869

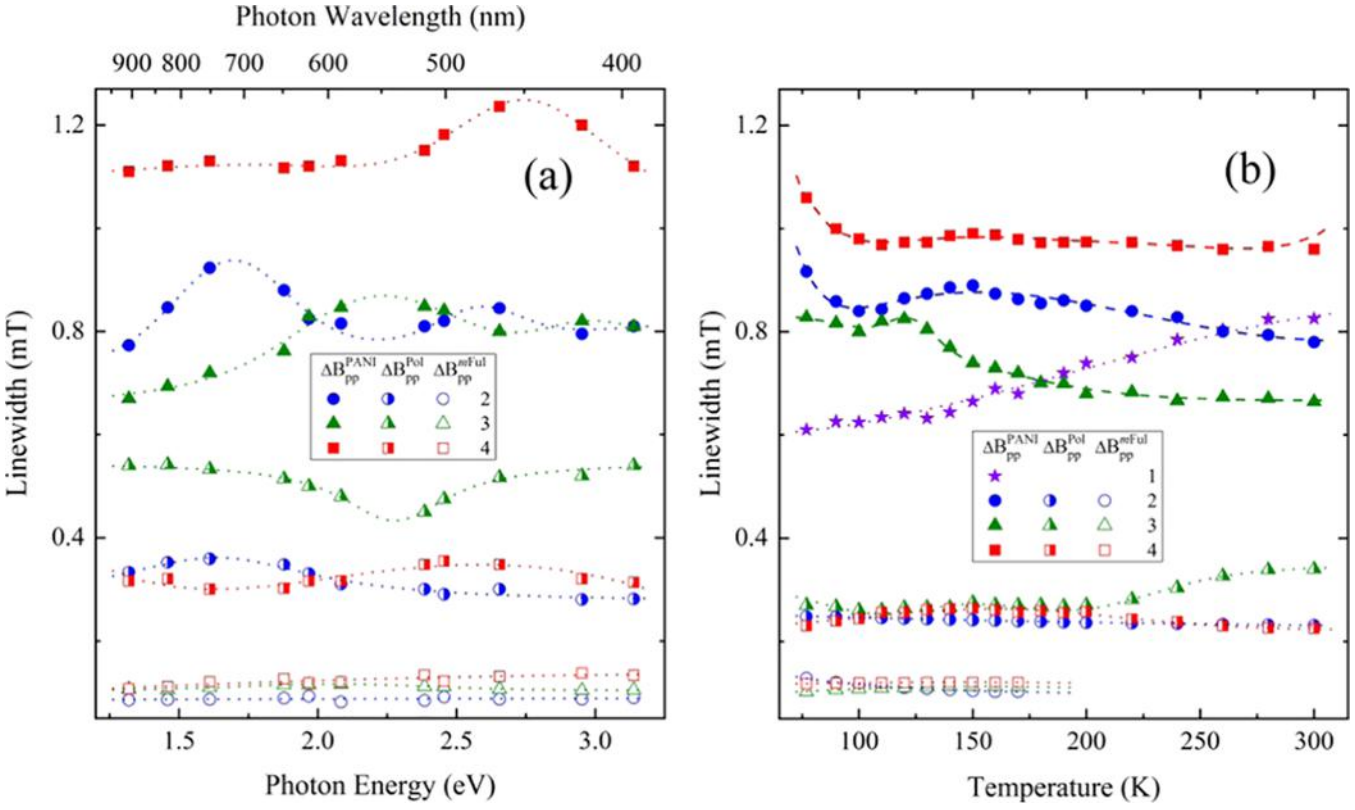

Figure 9. Effective line width of polarons $P^{+\bullet}_{PANI}$ stabilized in the PANI:TSA subsystem, ΔB^{PANI}_{pp}, (1), polarons $P^{+\bullet}$ and methanofullerene radical anions $mF^{-\bullet}_{mob}$, ΔB^{P}_{pp} and ΔB^{mF}_{pp}, respectively, photoinitiated in the F8T2:PC_{61}BM (2), PFO-DBT:PC_{61}BM (3), and PCDTBT:PC_{61}BM (4) subsystems as a function of photon energy $h\nu_{ph}$ at T = 77 K (a) and temperature at CCT T_c = 5500 K (b). Top-down dashed lines in (b) show dependences calculated from eq 2 with E_a = 0.062, 0.075, and 0.025, respectively, and J_{ex} = 0.044 eV. The dotted lines are drawn arbitrarily only for illustration to guide the eye.

where χ_0 is a constant, $\alpha = (3/2)J_{ex}/h\nu_{hop}$, J_{ex} is the amplitude of spin exchange during their collision and intrachain hopping diffusion with the rate $\nu_{hop} = \nu^0_{hop}\exp(-E_a/k_BT)$, ν^0_{hop} is a prefactor, k_B is the Boltzmann constant, and h is the Planck constant.

Temperature dependences calculated for the parameter n^{mF}_{mob}/n^{P}_{loc} of charge carriers photoinitiated in the samples under study are also shown in Figure 8b. It can be seen from the figure that the data obtained experimentally for the PANI:TSA/F8T2:PC_{61}BM, PANI:TSA/PFO-DBT:PC_{61}BM, and PANI:TSA/PCDTBT:PC_{61}BM dual-polymer composites are well approximated by the dependences calculated within the framework of the above approach from eq 1 with ΔE_{ij} = 0.034 eV and E_a = 0.019 eV, ΔE_{ij} = 0.072 eV and E_a = 0.037 eV, and ΔE_{ij} = 0.023 eV and E_a = 0.012 eV, respectively, and J_{ex} = 0.093 eV. The latter value lies near J_{ex} = 0.110 eV determined for P3DDT:PC_{61}BM BHJ[69] and the typical energy of polaron formation in π-conjugated polymers, $E_p \approx 0.1$ eV.[74] It is seen that both the energetic parameters obtained for mobile charge carriers decrease in the subsystem series PFO-DBT:PC_{61}BM → F8T2:PC_{61}BM → PCDTBT:PC_{61}BM. This directly correlates with the order of the recombination process carried out in these monopolymer composites and inversely correlates with their effective dimensionality.[42] Therefore, it could be concluded that the exchange interaction indeed increases in multispin composites, which facilitates the transfer of the charge and inhibits its recombination.

3.5. Line Width of Spin-Charge Carriers. The line width of LEPR spectra is the other important magnetic resonance parameter that reflects spin spatial distribution in the composite bulk and its static and dynamic interaction with its own microenvironment and other spin ensembles.[23] There are various factors leading to the broadening of spectral contributions of the paramagnetic centers stabilized or/and photoinitiated in multispin disordered systems, e.g., the weak anisotropy of their g-factor and their interaction with other spin-charge carriers. To determine separately line widths of all spin-charge carriers and analyze them at a wide range of experimental conditions, the effective LEPR spectra were deconvoluted.

Peak-to-peak line widths of polarons $P^{+\bullet}_{PANI}$ stabilized in the PANI:TSA subsystem and ΔB^{PANI}_{pp}, polarons $P^{+\bullet}_{loc}$, and methanofullerene radical anions $mF^{-\bullet}_{mob}$ photoinitiated in the F8T2:PC_{61}BM, PFO-DBT:PC_{61}BM, and PCDTBT:PC_{61}BM copolymer subsystems at T = 77 K are shown in Figure 9a as a function of the photon energy $h\nu_{ph}$. These values determined for the samples illuminated by achromatic white light with different CCTs are also summarized in Table 1. Previously, it was observed[39,40] that line widths of polarons $P^{+\bullet}_{loc}$ and methanofullerene radical anions $mF^{-\bullet}_{mob}$ photoinitiated in the PFO-DBT:PC_{61}BM BHJ are changed weakly with the photon energy $h\nu_{ph}$. On the other hand, the same parameters obtained for the same charge carriers photoinitiated in the F8T2:PC_{61}BM and PCDTBT:PC_{61}BM BHJ appeared to be more sensitive to the photon energy. The line widths of these centers change nonlinearly with $h\nu_{ph}$ and reach maximum values around 2.6, 2.1 and 2.4, 2.1 eV, respectively.[39−41] It must be emphasized that this picture changes sufficiently when

https://dx.doi.org/10.1021/acs.jpcc.0c02317
J. Phys. Chem. C 2020, 124, 10852−10869

these monopolymer narrow-band-gap composites are incorporated with the PANI:TSA subsystem. The analysis of the data presented in Figure 9a has testified a weak dependence of the line width of LEPR components on the photon energy $h\nu_{ph}$. One may note only slight broadening of the lines of polarons $P^{+\bullet}_{PANI}$ stabilized in the PANI:TSA subsystem near 2.8 eV and polarons $P^{+\bullet}_{loc}$ photoinitiated in the F8T2:$PC_{61}BM$ subsystem around 1.7 eV. Such leveling of sensitivity of the spectral line to the photon energy may be as a result of the change in the interaction between spins in both the copolymer and PANI backbones.

Let us analyze how the line width of LEPR spectra depends on the temperature. There are various temperature-dependent interactions causing the broadening of intrinsic EPR spectra of spin ensembles, the strongest of which are magnetic dipole−dipole and Heisenberg exchange interactions.[5] Assuming the general nature of spin-exchange interactions in condensed matter, one can write the following equation for the line width of the EPR spectrum[75]

$$\Delta B_{pp} = \Delta B^{0}_{pp} + \Delta B^{dd}_{pp} n_i \exp\left(\frac{E_a}{k_B T}\right) + \Delta B^{ex}_{pp} n_i \exp\left(-\frac{E_a}{k_B T}\right) \quad (2)$$

where $\Delta B^{0}_{pp} = 2/\sqrt{3}\gamma_e T_2$ is the intrinsic line width of a single spin randomly diffusing in the inhomogeneous copolymer backbone and unresolved hyperfine coupling with environmental nuclear spins; γ_e is the hydromagnetic ratio; ΔB^{dd}_{pp} and ΔB^{ex}_{pp} are the prefactors of the terms, which describe the broadening due to the spin dipole−dipole coupling and exchange interaction, respectively; n_i is the number of guest spins per copolymer unit; and E_a is the energy required for the translational spin movements in the copolymer backbone. The intrinsic line width mainly depends on the frequency-independent hyperfine spin interaction. It should be noted that the line width of spin-charge carriers photoinitiated in the samples under study also contains field-dependent terms due to the anisotropy of their g-factors (g-strain), which, however, are too small in the X-band EPR and, therefore, may not be taken into account. It seems quite obvious that the two last terms of eq 2 should determine a different dependence of the line width on temperature. Normally, the exchange interaction between polarons with $S = 1/2$ in conducting polymers is much stronger than the competing dipole−dipole coupling, i.e., $\Delta B^{dd}_{pp} \ll \Delta B_{pp}{}^{ex} = \alpha^2/2(1 + \alpha^2)$.[72] If the ratio J_{ex}/h exceeds the frequency of spin collision, then the regime of strong interaction is realized in the system, leading to a direct relation of the spin−spin interaction and polaron diffusion frequency, $\lim_{J_{ex}\to\infty} (\gamma_e \Delta B^{ex}_{pp} = n_i \nu_{hop})$. In an opposite case, the condition of weak interaction occurs in the system, resulting in an inverse dependence of these frequencies, $\lim_{J_{ex}\to 0} (\gamma_e \Delta B^{ex}_{pp}) = (n_i/\nu_{hop})(J_{ex}/h)^2$. According to the spin-exchange fundamental concepts,[71] the extremal character of the resulting temperature dependency with characteristic temperature T_c should evidence the realization of both types of spin−spin interaction at $T \le T_c$ and $T \ge T_c$. Thus, the broadening stipulated by the former interaction should be proportional to the ν_{hop} or ν^{-1}_{hop} values at the strong or weak spin-exchange limits, respectively, which leads to the appearance of an extreme contribution in respective dependences.[25,69]

Figure 9b shows the line widths of the polarons $P^{+\bullet}_{PANI}$ and $P^{+\bullet}_{loc}$ as well as of methanofullerene radical anions vs temperature. However, it is seen from the figure that the line widths of both $P^{+\bullet}_{loc}$ and $mF^{-\bullet}_{mob}$ radicals photoinitiated in all dual-polymer composites demonstrate a weak temperature dependence. This is consistent with the respective data obtained for all spin-charge carriers photoinitiated in the respective copolymer:methanofullerene composites, except for those obtained for polarons localized in the PFO-DBT:$PC_{61}BM$ composite whose temperature dependence contains a bell-like contribution with the extreme point lying near $T = 120$ K.[42] On the other hand, the EPR line of polarons $P^{+\bullet}_{PANI}$ stabilized in the PANI:TSA subsystem broadens monotonously with temperature as it was observed for its former state.[76] However, the line width begins to change appositively with temperature upon incorporation of this subsystem with photovoltaic BHJ. This is accompanied by the appearance on this dependence of an additional contribution, which reaches the maximum near $T = 120$ K in the case of PANI:TSA/PFO-DBT:$PC_{61}BM$ BHJ and $T < 80$ K in the case of the other samples. The analogous effect was also registered in the study of various multispin systems[34] including PCDTBT:$PC_{61}BM$[38] and PFO-DBT:$PC_{61}BM$[42] copolymer composites.

Temperature dependences, calculated from eq 2, are also shown in Figure 9b. It can be seen that the experimental data obtained for dual-polymer composites with the F8T2, PFO-DBT, and PCDTBT copolymer backbones can be well described in terms of the above approach with $E_a = 0.075$, 0.025, and 0.062 eV, respectively, and $J_{ex} = 0.044$ eV.

3.6. Relaxation and Dynamics of Spin-Charge Carriers. As the power of the microwave field increases in the cavity, the line width LEPR spectra broaden and their intensity first increases linearly, plateaus, and then decreases. This occurs due to the registering of the spectra at the steady-state MW saturation regime. Because polarons and methanofullerene radical anions previously bonded to the former excitons quickly spread far apart, they become independent, which allows us to use such effects for separate estimation of their spin−lattice T_1 and spin−spin T_2 relaxation times. EPR spectroscopy was used for determination of these parameters of spin-charge carriers stabilized and photoinitiated in different polymer systems[22,34] including various narrow-band-gap copolymer:methanofullerene composites.[39−42] Relaxation parameters are also important because they provide information about the interaction of paramagnetic centers with other radicals, as well as with their microenvironment. Besides, mobile spins induce an additional magnetic field at their location. The strength of this field is determined by the electronic relaxation, number, and dynamics of these paramagnetic centers. Since the charge carriers are characterized by different magnetic resonance parameters determined from the deconvolution of their effective LEPR spectrum, it also becomes possible to determine separately their dynamic parameters.

Relaxation parameters of spin ensembles in organic solids can be determined by registering their spectra at their steady-state MW saturation.[53,53]Figure S6 demonstrates how change amplitudes of spectral lines of spin-charge carriers stabilized or/and photoinitiated, e.g., in the dual-polymer PANI:TSA/PCDTBT:$PC_{61}BM$ BHJ under study on increasing the magnetic term B_1 of the MW field. Earlier it was shown[39−41] that the spin−spin relaxation time T_2 of both charge carriers formed in monopolymeric photovoltaic composites used in the present work as subsystems depends weakly on the energy of initiating photons. The same feature was analyzed to be

https://dx.doi.org/10.1021/acs.jpcc.0c02317
J. Phys. Chem. C 2020, 124, 10852−10869

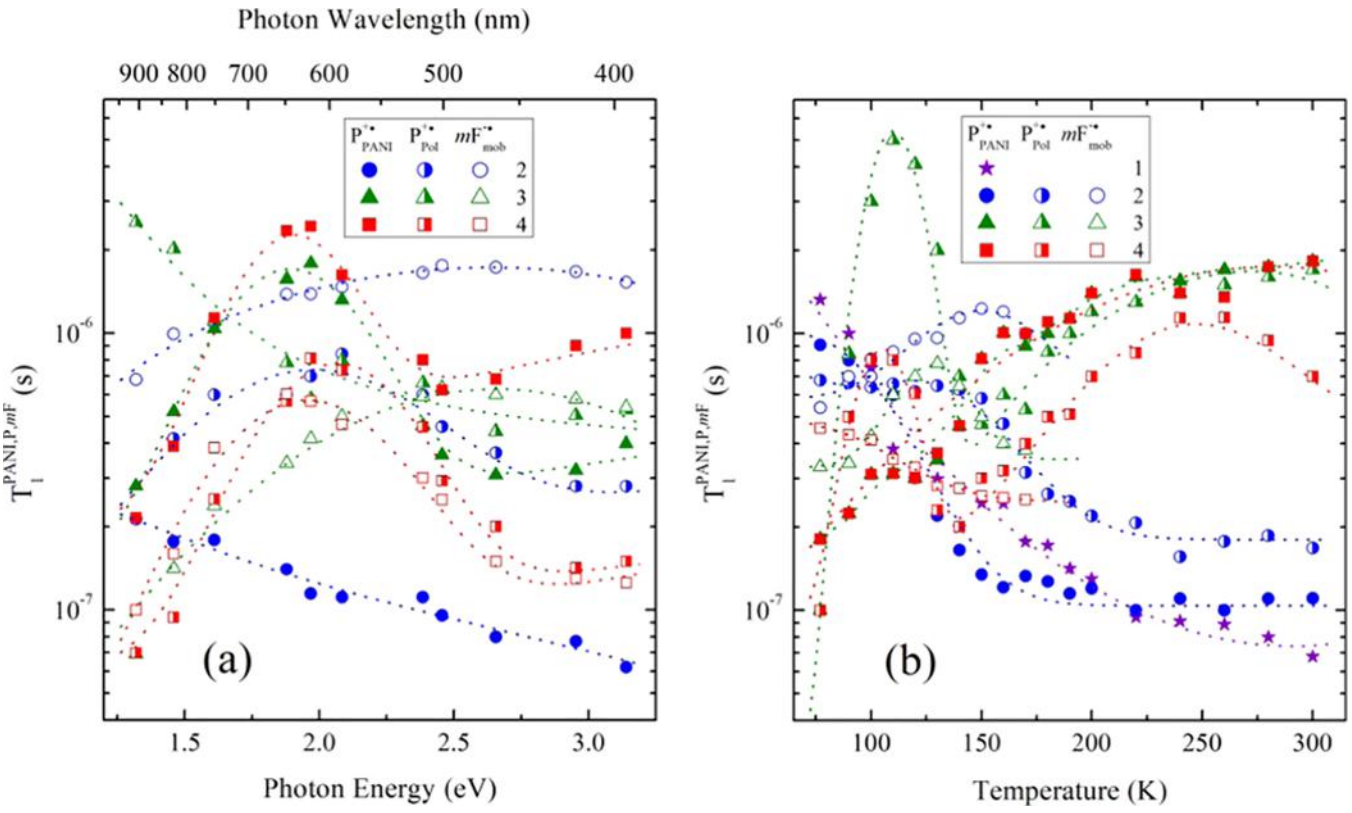

Figure 10. Spin−lattice relaxation times of polarons $P^{+\bullet}_{PANI}$, T_1^{PANI}, stabilized in the PANI:TSA subsystem (1), mobile and captured polarons $P^{+\bullet}$, T_1^{P}, as well as methanofullerene radical anions $mF^{-\bullet}_{mob}$, T_1^{mF}, photoinitiated in the F8T2:PC_{61}BM (2), PFO-DBT:PC_{61}BM (3), and PCDTBT:PC_{61}BM (4) subsystems as a function of photon energy $h\nu_{ph}$ at T = 77 K (a) and temperature at CCT T_c = 5500 K (b).

characteristic also after their incorporation into the PANI:TSA subsystem. This is why the results related to the study of spin−lattice relaxation and dynamic parameters of spin carriers, stabilized and photoinitiated in dual-polymer composites, have been discussed next.

Figure 10a depicts the dependence of the spin−lattice relaxation times of polarons $P^{+\bullet}_{PANI}$, T_1^{PANI} stabilized in the PANI:TSA subsystem, mobile and captured polarons $P^{+\bullet}$, T_1^{P}, as well as methanofullerene radical anions $mF^{-\bullet}_{mob}$, T_1^{mF}, photoinitiated in the copolymer subsystems on the energy of initiating photons $h\nu_{ph}$ determined using the steady-state MW saturation method. The presented data clearly indicate a dependence of spin−lattice relaxation of most charge carriers on the photon energy. As can be seen from the figure, spin−lattice relaxation of polarons $P^{+\bullet}_{PANI}$ in the sample PANI:TSA/F8T2:PC_{61}BM and $P^{+\bullet}$ in PANI:TSA/PFO-DBT:PC_{61}BM BHJ is monotonically accelerated with the $h\nu_{ph}$ increasing. This is accompanied by a monotonous increase in the T_1 parameter of photoinitiated methanofullerine radical anions. However, the main peculiarity of the data presented is the dependence of this parameter of other spin-charge carriers on the photon energy reaching a characteristic maximum at $h\nu_{ph} \approx 2.0$ eV. Because the band gap of PANI salt normally lies near or exceeds 4 eV,[77] this effect can rather be associated with the $\pi-\pi^*$ transition of the samples with a close optical band gap. A comparative analysis of the data obtained earlier[39−41] and in the present work showed that the spin−lattice relaxation of polarons and radical anions excited in the photovoltaic composites becomes less sensitive to the number and energy of photons when combined with the PANI:TSA subsystem. This may be due to a change in the exchange interaction between these spin subsystems with such a combination. It can additionally be caused by the release of part of the localized polarons from deep spin traps upon their interaction with corresponding photons.

Figure 10b shows how the time of spin−lattice relaxation of both the polarons $P^{+\bullet}_{PANI}$ and $P^{+\bullet}$, as well as methanofullerene radical anions $mF^{-\bullet}_{mob}$, changes when the samples are heated. As can be seen from the figure, spin−lattice relaxation of polarons stabilized in the PANI:TSA system is monotonically accelerated with the heating of this subsystem, which is typical for organic disordered semiconductors.[22] This dependence slightly changes when this subsystem is combined with the photovoltaic F8T2:PC_{61}BM one into the respective dual-polymer composite. Figure 9b, however, evidences, that once the F8T2:PC_{61}BM subsystem is replaced in the latter by the PFO-DBT:PC_{61}BM and PCDTBT:PC_{61}BM ones, electron relaxation of these polarons is accelerated at low temperatures and slowed down when the corresponding dual-polymer composite is heated. Such a change in the dependence slope can be explained by the difference in their structure and ordering that governs the interchain spin interaction, polaron ↔ bipolaron balance, or/and polaron realizing from high-energetic spin traps upon interaction with lattice phonons.

The temperature dependence of spin−lattice relaxation of polarons initiated in photovoltaic subsystems demonstrates a similar tendency. Indeed, the analysis of the data presented in Figure 10b shows some acceleration of electronic relaxation in the F8T2:PC_{61}BM subsystem when it is heated. When the PFO-DBT:PC_{61}BM and PCDTBT:PC_{61}BM subsystems are heated, this parameter of polarons increases, reaches their own extrema at T = 110 and 105 K, respectively, and then continues

https://dx.doi.org/10.1021/acs.jpcc.0c02317
J. Phys. Chem. C 2020, 124, 10852−10869

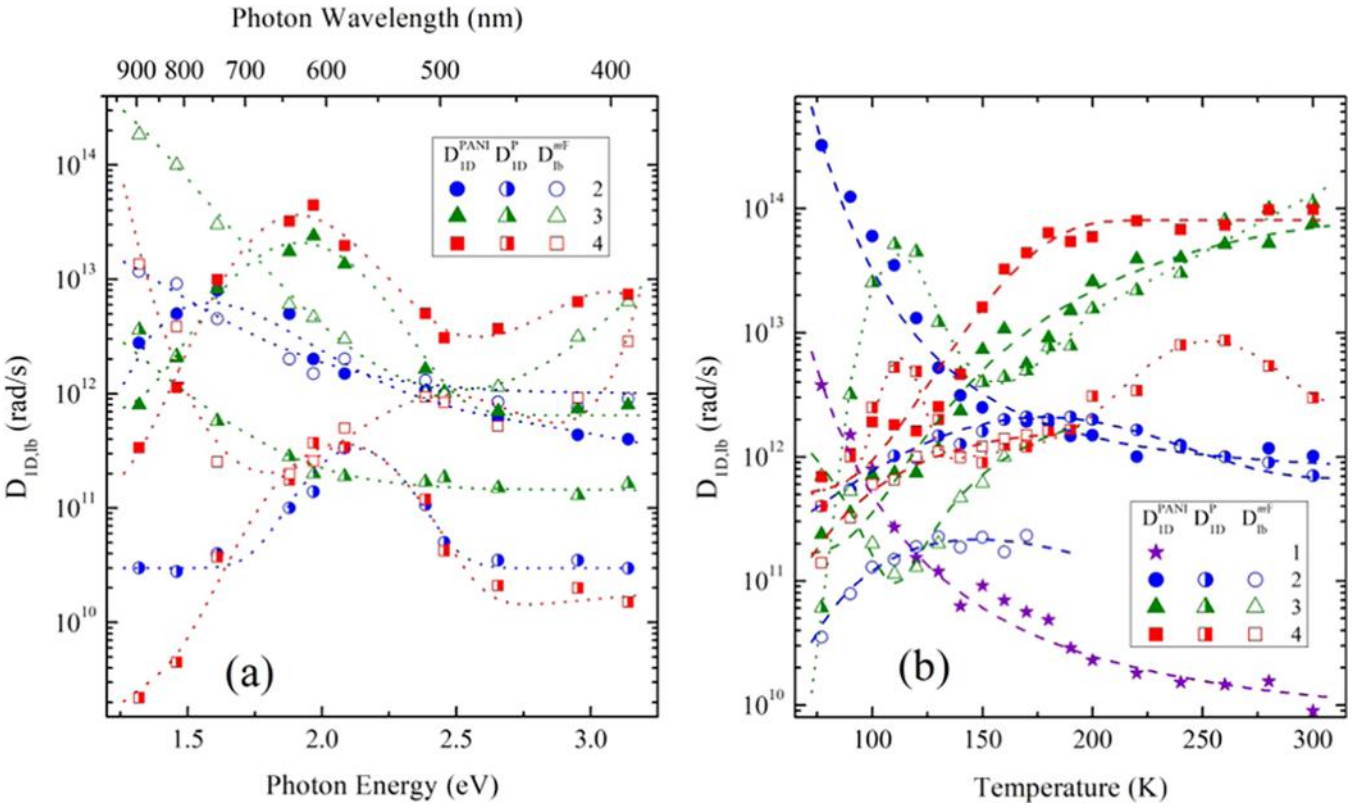

Figure 11. Translational diffusion coefficients of polarons $P_{PANI}^{+\bullet}$, hopping along the PANI chains (D_{1D}^{PANI}, filled points) in the PANI:TSA subsystem (1), polaron $P_{mob}^{+\bullet}$ intrachain hopping (D_{1D}^{P}, semifilled points) and librational rotation of methanofullerene radical anions $mF_{mob}^{-\bullet}$ (D_{lb}^{mF}, open points) photoinitiated in the F8T2:$PC_{61}BM$ (2), PFO-DBT:$PC_{61}BM$ (3), and PCDTB*T*:$PC_{61}BM$ (4) subsystems as a function of photon energy $h\nu_{ph}$ at T = 77 K (a) and temperature at CCT T_c = 5500 K (b). The error does not exceed the square of the points. The dashed lines connecting in (b) the filled star and circle experimental points were calculated from eq 4 with E_{ph} = 0.054 and 0.071 eV, respectively. The dashed lines connecting there the filled triangle and square experimental points were calculated from eq 5 with n_1 = 0.29, E_a = 0.067 eV and n_1 = 0.44, E_a = 0.060 eV, respectively. The dashed line connecting the semifilled circle experimental points was calculated from eq 5 with n_1 = 0.78, E_a = 0.055 eV. The dashed lines connecting the open circle, triangle, and square experimental points were calculated from eq 5 with n_1 = 0.55 and E_a = 0.036 eV, n_1 = 0.19 and E_a = 0.013 eV, and n_1 = 0.19 and E_a = 0.024 eV, respectively. The other dotted lines are drawn arbitrarily only for illustration to guide the eye.

to increase at higher temperatures. On the other hand, it has been shown previously[42] that the spin−lattice relaxation time of polarons photoinitiated in the initial composite F8T2:$PC_{61}BM$ is weakly temperature dependent, while this parameter of polarons is reduced by several times when the PFO-DBT:$PC_{61}BM$ and PCDTBT:$PC_{61}BM$ composites are cooled down over the entire temperature range.

The time of spin−lattice relaxation of methanofullerene radical anions photoinitiated in subsystems F8T2:$PC_{61}BM$ and PCDTBT:$PC_{61}BM$ increases and decreases, respectively, with their heating (Figure 10b). It is important to note that this occurs antibathically with the relaxation behavior of polarons stabilized in the respective PANI:TSA subsystem. Therefore, one can conclude that the exchange interaction of these charge carriers interconnects their relaxation processes in the above dual-polymer composites. At the same time, the parameter T_1 of the carriers of the negative charge in subsystem PFO-DBT:$PC_{61}BM$ demonstrates an extreme character with a maximum around T = 130 K. This might be evidence of their lesser interaction with the spin ensemble of another subsystem. So, one may point out a complex dependence of spin relaxation on the structure and ordering of its environment as well as on its exchange interaction with other spin ensembles resulting from possible polaron−bipolaron transition or/and polaron realizing from high-energetic spin traps upon photon−phonon interaction.

There are different spin-assisted dynamic processes realized in the polymer:fullerene composites, namely, polaron diffusion along the polymer chains with coefficient D_{1D}, its hopping between polymer chains with coefficient D_{3D}, and librational rotation diffusion of fullerene radical anions around the main molecular axis with coefficient D_{lb}. These parameters can be determined from the concentration-broadening of EPR spectra of paramagnetic centers in condensed systems,[71] especially at different wavebands EPR.[19,23] Because spin dynamic processes induce additional magnetic fields in the place of location of electron and nuclear spins, which accelerate their relaxation, this allows one to determine more accurately dynamic parameters of different spin ensembles. The fluctuations of the lattice of conjugated polymers are normally faster than the fluctuations in the decaying macroscopic magnetization.[19] Besides, the relation $T_1 \geq T_2$ is always true for spin-charge carriers in such systems.[34] This means that the systems under study are in the Redfield regime and all relaxation processes can be described in terms of the respective theory of spin relaxation.[78,79] Taking into account the fact that the relaxation is defined mainly by a dipole−dipole interaction of spins with its own environment, the relation connecting relaxation and dynamic processes can be written as[80]

$$T_1^{-1}(\omega_e) = \langle \omega^2 \rangle [2J(\omega_e) + 8J(2\omega_e)] \quad (3)$$

https://dx.doi.org/10.1021/acs.jpcc.0c02317
J. Phys. Chem. C 2020, 124, 10852−10869

where $\langle\omega^2\rangle = 1/10\ \gamma_e^4\hbar^2S(S+1)n\sum_{ij}$ is a constant of a dipole−dipole interaction for powder; n is a spin density in each polymer unit; $\sum_{ij}$ is the lattice sum for a powderlike sample; $J(\omega_e)=(2D^{|}_{1D}\ \omega_e)^{-1/2}$ (at $D^{|}_{1D} \gg \omega_e \gg D_{3D}$) and $J(\omega_e) = \tau_c/(1 + \tau_c^2\omega_e^2)$ are spectral density functions for Q1D longitudinal and rotational isotropic libration diffusion with correlation time τ_c, respectively;[19,81] $D^{|}_{1D} = 4D_{1D}/L^2$; ω_e is resonant angular frequency of the electron spin precession; and L is a factor of spin delocalization over a polaron equal, e.g., to three PCDTBT units.[35,50] The latter value was used for calculation of spin dynamic parameters in the initial copolymer composites[42] and, in these compounds, used in the dual-polymer composites under study as respective photovoltaic subsystems.

The above-mentioned dynamic parameters calculated for the samples under study from eq 3 with the data presented in Figure 10 are shown in Figure 11 as functions of the photon energy and temperature. The same parameters determined for these composites illuminated by achromatic white light with different CCTs are also summarized in Table 1.

Earlier, it was shown[39−41] that dynamics of polarons in the F8T2:$PC_{61}BM$ and PFO-DBT:$PC_{61}BM$ composites weakly depends on the photon energy, whereas librational rotation dynamics of methanofullerene radical anions depends on the photon energy reaching the maximum value at ca. 1.9 and 2.7 eV. Because $D_{lb}^{mF} \propto 1/nT_1^{mF}$ (see eq 3), the dynamics of these charge carriers may be governed by their recombination with oppositely charged polarons as well as by their possible formation from bipolarons and realizing from spin traps upon interaction with the lattice phonons mentioned above. The analogous conclusion may be made for diffusion dynamics of polarons whose diffusion coefficient follows the stronger relation $D_{1D}^{P} \propto (nLT_1^{P})^2$. When the above matrices are replaced by the PCDTBT one, these dynamic parameters become stronger to depend on the photon energy demonstrating respective extremes around 1.7 eV. Such dissimilarity was explained by the different number and spatial distribution of spin traps formed in these composites with differently disordered matrices. This is changed drastically once these monopolymer composites are associated with the PANI:TSA subsystem. As shown in Figure 10a, this leads to sufficient leveling of their extremities. One should note the conjoint respective dependences of the polaron diffusion rate in the photovoltaic subsystem F8T2:$PC_{61}BM$ of the respective composite PANI:TSA/F8T2:$PC_{61}BM$, in the subsystem PANI:TSA of the dual-polymer composite PANI:TSA/PFO-DBT:$PC_{61}BM$, as well as in both polymeric subsystems of the PANI:TSA/PCDTBT:$PC_{61}BM$ dual-polymer composite with an extremal characteristic energy lying near 2.0 eV. This should indicate that spin-exchange interaction originated in a photovoltaic composite on its association with the guest PANI:TSA subsystem leads to the leveling of the sample selectivity/sensitivity to the light photon energy, which increases the number of photons absorbed by such dual-polymer composites and, therefore, its efficiency of light energy conversion.

Heating of the samples accelerates not only the electron relaxation of charge carriers but also other spin-assisted processes of charge separation, transfer, interaction, and recombination. Figure 11b shows the temperature dependences of respective diffusion coefficients of all spin-charge carriers stabilized and initiated in the dual-polymer composites under study upon their irradiation by white light with CCT of T_c = 5500 K. The analysis of experimental data has shown that the charge is transferred through the PANI:TSA matrix according to the approach of polaron interaction with the lattice phonons[82]

$$D_{1D} = D_{1D}^{0}T\left[\left(\exp\left(\frac{E_{ph}}{k_BT}\right) - 1\right)\left(1 - \exp\left(\frac{E_{ph}}{k_BT}\right)\right)\right] \quad (4)$$

where D_{1D}^{0} is a constant and E_{ph} is the energy of lattice phonons. As follows from the figure, the experimental dependence can be well described within the above approach at E_{ph} = 0.054 eV. Once the PANI:TSA subsystem combines with the F8T2:$PC_{61}BM$ one, this parameter increases up to 0.071 eV. Such a mechanism changes when the F8T2 backbone of the dual-polymer composite is replaced by the PFO-DBT or PCDTBT ones. In this case, the charge seems more likely to be transferred within the framework of polaron activation hopping through the respective copolymer BHJ with the diffusion coefficient[83,84]

$$D_{1D} = D_{1D}^{0}T^2\nu_e^{s}\exp\left(\frac{E_a}{k_BT}\right) \quad (5)$$

where $s = 1 - n_1k_BT/E_a$, n_1 is a constant, and E_a is the energy for activation of the charge carrier to extended states. Indeed, Figure 11b evidences that the dynamics of polarons stabilized in the PANI:TSA backbone of the PANI:TSA/PFO-DBT:$PC_{61}BM$ and PANI:TSA/PCDTBT:$PC_{61}BM$ dual-polymer composites follows eq 5 with E_a = 0.067 and 0.060 eV, respectively. The analysis of the data obtained shows that the dynamics of polarons diffusing in subsystem F8T2:$PC_{61}BM$ can also be described within this activation mechanism with E_a = 0.055 eV. The dynamics of these charge carriers becomes more complicated when replacing this subsystem with PFO-DBT:$PC_{61}BM$ and PCDTBT:$PC_{61}BM$ ones. Figure 11b shows that in the temperature dependences of the respective dual-polymer composites described by eq 5 with E_a = 0.084 and 0.087 eV, respectively, there appears an extreme contribution with a characteristic point around T = 115 K. The emergence of such a contribution may be caused by the better ambipolarity of these copolymer matrices and, as a result, a more specific exchange interaction between spin ensembles formed in respective dual-polymer composites. The libration mobility of the methanofullerene radical anions in the PANI:TSA/F8T2:$PC_{61}BM$, PANI:TSA/PFO-DBT:$PC_{61}BM$, and PANI:TSA/PCDTBT:$PC_{61}BM$ dual-polymer composites was analyzed to follow also eq 5 with E_a = 0.036, 0.013, and 0.024 eV, respectively (Figure 11b).

4. CONCLUSIONS

In this work, we first performed comparative LEPR studies of different spin-assisted processes carried out in dual-polymer multispin composites PANI:TSA/F8T2:$PC_{61}BM$, PANI:TSA/PFO-DBT:$PC_{61}BM$, and PANI:TSA/PCDTBT:$PC_{61}BM$. Illumination of these composites by NIR−vis−UV light leads to fast spin-charge formation, separation, diffusion, and recombination in their narrow-band-gap copolymer:methanofullerene subsystems. As expected, the effective LEPR spectra of dual-polymer composites appeared to consist of respective contributions due to polarons $P^{+\bullet}_{PANI}$ stabilized in the PANI backbone, polarons $P^{+\bullet}_{loc}$ captured by deep spin traps that are formed in copolymer matrices due to their disordering, as well

https://dx.doi.org/10.1021/acs.jpcc.0c02317
J. Phys. Chem. C 2020, 124, 10852−10869

as to mobile pairs of polarons and methanofullerene radical anions, $P^{+\bullet}_{mob} \leftrightarrow mF^{-\bullet}_{mob}$, photoinitiated in the photovoltaic subsystem. A part of polarons formed in adjacent polymer chains can combine into bipolarons with equal *g*-factors and double elemental charge. Besides, some immobilized polarons can be realized from high-energetic spin traps upon interaction with light photons or/and lattice phonons. This should be taken into account when interpreting the effective LEPR spectra of the systems under study and all spin-assisted processes being carried out in them.

The number and dynamics of charge carriers photoinitiated in the photovoltaic subsystem are determined by structure, morphology, and also by the density and energy of the initiating light photons. They appeared to be more sensitive to the light photons of a definite energy band. This effect may occur as a result of an exchange interaction between different spin ensembles in the dual-polymer composites and can be used for creation, e.g., of optical converters and filters. The contribution of mobile charge carriers to the LEPR spectra of dual-polymer composites decreases exponentially with increasing temperature due to their accelerated recombination. This process was interpreted within the framework of tunneling of spin-charge carriers along copolymer chains of photovoltaic subsystems and their exchange interaction with other spin ensembles. Such an interaction thus optimizes the molecular properties of multispin dual-polymer composites, facilitates the transfer of charges, and inhibits their recombination.

The results obtained allow us to conclude the crucial role of exchange interaction between different spin ensembles in all processes occurring in multispin polymer composites. By changing this interaction at a certain physical influence, one could handle electronic properties and functionalities of multispin organic systems. Spin interaction eliminates the selectivity of the multispin system to the photon energy, extends the range of optical photons absorbed by multispin dual-polymer composites, and, therefore, increases its efficiency to converse the light energy.

■ ASSOCIATED CONTENT

Supporting Information

The Supporting Information is available free of charge at https://pubs.acs.org/doi/10.1021/acs.jpcc.0c02317.

NIR−vis−UV spectra of the F8T2:PC_{61}BM, PFO-DBT:PC_{61}BM, and PCDTBT:PC_{61}BM copolymer composites as well as the PANI:TSA/F8T2:PC_{61}BM, PANI:TSA/PFO-DBT:PC_{61}BM, and PANI:TSA/PCDTBT:PC_{61}BM dual-polymer composites, registered at T = 298 K (Figure S1); denomination of the atom number of the $\pi-\pi$ stacking 4ANI/2CDTBT complex after MM2 steric energy optimization (Figure S2); model of the $\pi-\pi$ stacking (8ANI:2TSA/ CDTBT) complex after MM2 optimization (Figure S3); CTDTBT monomer with a $-(CH_2)_3-CH_3$ side chain (Figure S4); CTDTBT monomer with a $(-CH_3)$ side chain (Figure S5); intensity of EPR lines of polarons stabilized on the PANI chains, polarons initiated by photons with $h\nu_{ph}$ = 1.97 eV on the PCDTBT chains as well as PC_{61}BM radical anions at T = 77 K as a function of the magnetic term B_1 of the MW field (Figure S6); complex model of 4ANI:2TSA/2CDTBT:PC_{61}BM (only FF energy/structure optimization) (Table S1); Cartesian coordinates of the 4ANI/2CDTBT system used for the DFT single point energy optimization in the Gaussian (G09W) package (Table S2); hfc parameters of ^1H atoms attributed to the same positions on monomer frames (Table S3) (PDF)

■ AUTHOR INFORMATION

Corresponding Author

Victor I. Krinichnyi − *Department of Kinetics and Catalysis, Institute of Problems of Chemical Physics RAS, Chernogolovka 142432, Russia;* orcid.org/0000-0002-5227-763X; Phone: +7(496-52)21882; Email: kivirus@gmail.com

Authors

Evgeniya I. Yudanova − *Department of Kinetics and Catalysis, Institute of Problems of Chemical Physics RAS, Chernogolovka 142432, Russia*

Nikolay N. Denisov − *Department of Kinetics and Catalysis, Institute of Problems of Chemical Physics RAS, Chernogolovka 142432, Russia*

Aleksei A. Konkin − *Center for Micro- and Nanotechnologies, Ilmenau University of Technology, D-98693 Ilmenau, Germany; Institute of Physics, Kazan Federal University, 420008 Kazan, Russia*

Uwe Ritter − *Center for Micro- and Nanotechnologies, Ilmenau University of Technology, D-98693 Ilmenau, Germany;* orcid.org/0000-0002-9315-4863

Bernhard Wessling − *BWIT e.K., D-22941 Jersbek, Germany*

Alexander L. Konkin − *Center for Micro- and Nanotechnologies, Ilmenau University of Technology, D-98693 Ilmenau, Germany;* orcid.org/0000-0002-2418-2676

Victor R. Bogatyrenko − *Department of Kinetics and Catalysis, Institute of Problems of Chemical Physics RAS, Chernogolovka 142432, Russia*

Complete contact information is available at: https://pubs.acs.org/10.1021/acs.jpcc.0c02317

Notes

The authors declare no competing financial interest.

■ ACKNOWLEDGMENTS

This work was performed in accordance with the State Assignment, No. AAAA-A19-119032690060-9, in part funded by the Russian Foundation for Basic Research, Grant no. 18-29-20011-mk, and supported by the DFG Project no. DFG RI966/15-1.

■ REFERENCES

(1) Tjong, S. C. *Polymer Composites with Carbonaceous Nanofillers: Properties and Applications*; Wiley-VCH Verlag: Weinheim, 2012.

(2) Zhang, G.; Manjooran, N. *Nanofabrication and Its Application in Renewable Energy*; The Royal Society of Chemistry, 2014.

(3) Petty, M. C. *Organic and Molecular Electronics: From Principles to Practice*, 2nd ed.; Wiley-Blackwell, 2019.

(4) Xu, Y.; Awschalom, D. D.; Nitta, J. *Handbook of Spintronics*; Springer-Verlag, 2015.

(5) Likhtenshtein, G. I. *Electron Spin Interactions in Chemistry and Biology: Fundamentals, Methods, Reactions Mechanisms, Magnetic Phenomena, Structure Investigation*; Springer, 2016.

(6) Brabec, C.; Scherf, U.; Dyakonov, V. *Organic Photovoltaics: Materials, Device Physics, and Manufacturing Technologies*, 2nd ed.; Wiley-VCH: Weinheim, 2014; Vol *1*.

(7) Tress, W. *Organic Solar Cells: Theory, Experiment, and Device Simulation*; Springer International Publishing, 2014.

(8) Huang, F.; Yip, H.-L.; Cao, Y., *Polymer Photovoltaics: Materials, Physics, and Device Engineering*. The Royal Society of Chemistry: Cambridge, 2015.
(9) Ostroverkhova, O. *Handbook of Organic Materials for Optical and (Opto)Electronic Devices: Properties and Applications*; Woodhead Publishing Ltd: Philadelphia, 2013; Vol. *39*.
(10) Zhao, L.; Zhao, S. L.; Xu, Z.; Gong, W.; Yang, Q. Q.; Fan, X.; Xu, X. R. Influence of Morphology of PCDTBT:PC71BM on the Performance of Solar Cells. *Appl. Phys. A: Mater. Sci. Process.* **2014**, *114*, 1361−1368.
(11) Banerji, N.; Cowan, S.; Leclerc, M.; Vauthey, E.; Heeger, A. J. Exciton Formation, Relaxation, and Decay in PCDTBT. *J. Am. Chem. Soc.* **2010**, *132*, 17459−17470.
(12) Liu, J. G.; Chen, L.; Gao, B. R.; Cao, X. X.; Han, Y. C.; Xie, Z. Y.; Wang, L. X. Constructing the Nanointerpenetrating Structure of PCDTBT:PC70BM Bulk Heterojunction Solar Cells Induced by Aggregation of PC70BM via Mixed-Solvent Vapor Annealing. *J. Mater. Chem. A* **2013**, *1*, 6216−6225.
(13) Gutzler, R.; Perepichka, D. F. π-Electron Conjugation in Two Dimensions. *J. Am. Chem. Soc.* **2013**, *135*, 16585−16594.
(14) Wang, T.; Lidzey, D. G. Bulk Heterojunction Morphology Characterization. In *Organic Solar Cells: Fundamentals, Devices, and Upscaling*, 1st ed.; Rand, B. P.; Richter, H., Eds.; CRC Press, Taylor & Francis Group: Boca Raton, 2014; pp 317−366.
(15) Yonezawa, K.; Ito, M.; Kamioka, H.; Yasuda, T.; Han, L. Y.; Moritomo, Y. Charge-Transfer State and Charge Dynamics in Poly(9,9'-Dioctylfluorene-co-Bithiophene) and 6,6 -Phenyl-C-70-Butyric Acid Methyl Ester Blend Film. *Appl. Phys. Express* **2011**, *4*, No. 122601.
(16) Lupton, J. M.; McCamey, D. R.; Boehme, C. Coherent Spin Manipulation in Molecular Semiconductors: Getting a Handle on Organic Spintronics. *ChemPhysChem* **2010**, *11*, 3040−3058.
(17) Davidov, D.; Moraes, F.; Heeger, A. J.; Wudl, F.; Kim, H.; Dalton, L. R. Electron-Spin Echo Modulation and Relaxation in Polythiophene. *Solid State Commun.* **1985**, *53*, 497−500.
(18) Mizoguchi, K. Spin Dynamics Study in Conducting Polymers by Magnetic-Resonance. *Jpn. J. Appl. Phys., Part 1* **1995**, *34*, 1−19.
(19) Mizoguchi, K.; Kuroda, S. Magnetic Properties of Conducting Polymers. In *Handbook of Organic Conductive Molecules and Polymers*; Nalwa, H. S., Ed.; John Wiley & Sons: Chichester, NY, 1997; Vol. *3*, pp 251−317.
(20) Uvarov, M. N.; Kulik, L. V. Electron Spin Echo of Photoinduced Spin-Correlated Polaron Pairs in P3HT:PCBM Composite. *Appl. Magn. Reson.* **2013**, *44*, 97−106.
(21) Kraffert, F.; Steyrleuthner, R.; Albrecht, S.; Neher, D.; Scharber, M. C.; Bittl, R.; Behrends, J. Charge Separation in PCPDTBT:PCBM Blends from an EPR Perspective. *J. Phys. Chem. C* **2014**, *118*, 28482−28493.
(22) Krinichnyi, V. I. 2-mm Waveband Electron Paramagnetic Resonance Spectroscopy of Conducting Polymers (Review). *Synth. Met.* **2000**, *108*, 173−222.
(23) Misra, S. K. *Multifrequency Electron Paramagnetic Resonance. Theory and Applications*; Wiley-VCH: Weinheim, 2011.
(24) Naveed, K.-u.-R.; Wang, L.; Yu, H.; Ullah, R. S.; Haroon, M.; Fahad, S.; Li, J.; Elshaarani, T.; Khan, R. U.; Nazir, A. Recent Progress in the Electron Paramagnetic Resonance Study of Polymers. *Polym. Chem.* **2018**, *9*, 3306−3335.
(25) Krinichnyi, V. I.; Roth, H. K.; Schrödner, M.; Wessling, B. EPR Study of Polyaniline Highly Doped by *p*-Toluenesulfonic Acid. *Polymer* **2006**, *47*, 7460−7468.
(26) Krinichnyi, V. I.; Tokarev, S. V.; Roth, H. K.; Schrödner, M.; Wessling, B. EPR Study of Charge Transfer in Polyaniline Highly Doped by *p*-Toluenesulfonic Acid. *Synth. Met.* **2006**, *156*, 1368−1377.
(27) Krinichnyi, V. I.; Yudanova, E. I.; Wessling, B. Influence of Spin−Spin Exchange on Charge Transfer in PANI-ES/P3DDT/PCBM Composite. *Synth. Met.* **2013**, *179*, 67−73.
(28) Krinichnyi, V. I. Dynamics of Spin Charge Carriers in Polyaniline. *Appl. Phys. Rev.* **2014**, *1*, No. 021305.
(29) Wessling, B. New Insight into Organic Metal Polyaniline Morphology and Structure. *Polymers* **2010**, *2*, 786−798.
(30) Brabec, C.; Dyakonov, V.; Parisi, J.; Sariciftci, N. S. *Organic Photovoltaic: Concepts and Realization*; Springer: Berlin, 2003.
(31) Marumoto, K.; Muramatsu, Y.; Kuroda, S. Quadrimolecular Recombination Kinetics of Photogenerated Charge Carriers in Regioregular Poly(3-Alkylthiophene)/Fullerene Composites. *Appl. Phys. Lett.* **2004**, *84*, 1317−1319.
(32) Sensfuss, S.; Konkin, A.; Roth, H. K.; Al-Ibrahim, M.; Zhokhavets, U.; Gobsch, G.; Krinichnyi, V. I.; Nazmutdinova, G. A.; Klemm, E. Optical and ESR Studies on Poly(3-Alkylthiophene)/Fullerene Composites for Solar Cells. *Synth. Met.* **2003**, *137*, 1433−1434.
(33) Krinichnyi, V. I., *Multi Frequency EPR Spectroscopy of Conjugated Polymers and Their Nanocomposites*; CRC Press, Taylor & Francis Group: Boca Raton, FL, 2016.
(34) Krinichnyi, V. I. EPR Spectroscopy of Polymer:Fullerene Nanocomposites. *Spectroscopy of Polymer Nanocomposites*, 1st ed.; Thomas, S.; Rouxel, D.; Ponnamma, D., Eds.; Elsevier: Amsterdam, 2016; pp 202−275, and the references therein
(35) Niklas, J.; Poluektov, O. G. Charge Transfer Processes in OPV Materials as Revealed by EPR Spectroscopy. *Adv. Energy Mater.* **2017**, *7*, No. 1602226.
(36) Konkin, A.; Popov, A.; Ritter, U.; Orlinskii, S.; Mamin, G.; Aganov, A.; Konkin, A. A.; Scharff, P. Combined W-Band Light-Induced ESR/ENDOR/TRIPLE and DFT Study of PPV-Type/PC61BM Ion Radicals. *J. Phys. Chem. C* **2016**, *120*, 28905−28911.
(37) Konkin, A.; Ritter, U.; Konkin, A. A.; Mamin, G.; Orlinskii, S.; Gafurov, M.; Aganov, A.; Klochkov, V.; Lohwasser, R.; Thelakkat, M.; et al. W-Band ENDOR of Light-Induced PPerAcr Anion Radicals in Double-Crystalline Donor−Bridge−Acceptor P3HT-b-PPerAcr Block Copolymer in Frozen Solution: Experimental and DFT Study. *J. Phys. Chem. C* **2018**, *122*, 22829−22837.
(38) Krinichnyi, V. I.; Yudanova, E. I.; Denisov, N. N. The Role of Spin Exchange in Charge Transfer in Low-Bandgap Polymer:-Fullerene Bulk Heterojunctions. *J. Chem. Phys.* **2014**, *141*, No. 044906.
(39) Krinichnyi, V. I.; Yudanova, E. I.; Bogatyrenko, V. R. Effect of Spin Traps on Charge Transport in Low-Bandgap Copolymer:Fullerene Composites. *J. Phys. Chem. Solids* **2017**, *111*, 153−159.
(40) Krinichnyi, V. I.; Yudanova, E. I.; Bogatyrenko, V. R. Effect of Spin Localization on Charge Transport in Low-Bandgap Bilayered Ordered Nanocomposites. *Sol. Energy Mater. Sol. Cells* **2018**, *174*, 333−341.
(41) Krinichnyi, V. I.; Yudanova, E. I.; Bogatyrenko, V. R. Light-Induced EPR Study of Spin-Assisted Charge Transport in PFOT:PC_{61}BM Composite. *J. Photochem. Photobiol., A* **2019**, *372*, 288−295.
(42) Krinichnyi, V. I.; Yudanova, E. I.; Denisov, N. N.; Bogatyrenko, V. R. Light-Induced Electron Paramagnetic Resonance Spectroscopy of Spin-Assisted Charge Transfer in Narrow-Bandgap Copolymer:-Methanofullerene Composites. *J. Phys. Chem. C* **2019**, *123*, 16533−16545.
(43) Kawai, T.; Okazaki, S.; Mizobuchi, H.; Araki, H.; Yoshino, K. Novel Ferromagnetic Behavior of Conducting Polymers Doped with Fullerene and TDAE. *Synth. Met.* **1997**, *86*, 2333−2334.
(44) Huang, J. H.; Yang, C. Y.; Ho, Z. Y.; Kekuda, D.; Wu, M. C.; Chien, F. C.; Chen, P. L.; Chu, C. W.; Ho, K. C. Annealing Effect of Polymer Bulk Heterojunction Solar Cells Based on Polyfluorene and Fullerene Blend. *Org. Electron.* **2009**, *10*, 27−33.
(45) Kato, T.; Hagiwara, N.; Suzuki, E.; Nasu, Y.; Izawa, S.; Tanaka, K.; Kato, A. Morphology Control for Highly Efficient Organic−Inorganic Bulk Heterojunction Solar Cell Based on Ti-Alkoxide. *Thin Solid Films* **2016**, *600*, 98−102.
(46) Park, S. H.; Roy, A.; Beaupre, S.; Cho, S.; Coates, N.; Moon, J. S.; Moses, D.; Leclerc, M.; Lee, K.; Heeger, A. J. Bulk Heterojunction Solar Cells with Internal Quantum Efficiency Approaching 100%. *Nat. Photonics* **2009**, *3*, 297−302.

https://dx.doi.org/10.1021/acs.jpcc.0c02317
J. Phys. Chem. C 2020, 124, 10852−10869

(47) Kim, D. H.; Song, H. J.; Heo, S. W.; Song, K. W.; Moon, D. K. Enhanced Photocurrent Generation by High Molecular Weight Random Copolymer Consisting of Benzothiadiazole and Quinoxaline as Donor Materials. *Sol. Energy Mater. Sol. Cells* **2014**, *120*, 94−101.
(48) Yoo, S. H.; Kum, J. M.; Cho, S. O. Tuning the Electronic Band Structure of PCBM by Electron Irradiation. *Nanoscale Res. Lett.* **2011**, *6*, 545−551.
(49) Poluektov, O. G.; Filippone, S.; Martín, N.; Sperlich, A.; Deibel, C.; Dyakonov, V. Spin Signatures of Photogenerated Radical Anions in Polymer-[70]Fullerene Bulk Heterojunctions: High Frequency Pulsed EPR Spectroscopy. *J. Phys. Chem. B* **2010**, *114*, 14426−14429.
(50) Niklas, J.; Mardis, K. L.; Banks, B. P.; Grooms, G. M.; Sperlich, A.; Dyakonov, V.; Beaupre̊, S.; Leclerc, M.; Xu, T.; Yue, L.; et al. Highly-Efficient Charge Separation and Polaron Delocalization in Polymer−Fullerene Bulk-Heterojunctions: A Comparative Multi-Frequency EPR and DFT Study. *Phys. Chem. Chem. Phys.* **2013**, *15*, 9562−9574.
(51) Krzystek, J.; Sienkiewicz, A.; Pardi, L.; Brunel, L. C. DPH as a Standard for High-Field EPR. *J. Magn. Reson.* **1997**, *125*, 207−211.
(52) Weil, J. A.; Bolton, J. R.; Wertz, J. E. *Electron Paramagnetic Resonance: Elementary Theory and Practical Applications*; Wiley-Interscience: New York, 2007; Vol. *2d*.
(53) Marumoto, K.; Takeuchi, N.; Ozaki, T.; Kuroda, S. ESR Studies of Photogenerated Polarons in Regioregular Poly(3-Alkylthiophene)-Fullerene Composite. *Synth. Met.* **2002**, *129*, 239−247.
(54) Dennany, L.; Innis, P. C.; McGovern, S. T.; Wallace, G. G.; Forster, R. J. Electronic Interactions within Composites of Polyanilines Formed under Acidic and Alkaline Conditions. Conductivity, ESR, Raman, UV-Vis and Fluorescence Studies. *Phys. Chem. Chem. Phys.* **2011**, *13*, 3303−3310.
(55) Tzou, K.; Gregory, R. V. A Method to Prepare Soluble Polyaniline Salt Solutions - *in Situ* Doping of PANI Base with Organic Dopants in Polar Solvents. *Synth. Met.* **1993**, *53*, 365−377.
(56) Zhang, Y.; Basel, T. P.; Gautam, B. R.; Yang, X. M.; Mascaro, D. J.; Liu, F.; Vardeny, Z. V. Spin-Enhanced Organic Bulk Heterojunction Photovoltaic Solar Cells. *Nat. Commun.* **2012**, *3*, No. 1043.
(57) Yang, M.; Xiang, Z.; Wang, G. A Novel Orchid-Like Polyaniline Superstructure by Solvent−Thermal Method. *J. Colloid Interface Sci.* **2012**, *367*, 49−54.
(58) Klebe, G.; Graser, F.; Hädicke, E.; Berndt, J. Crystallochromy as a Solid-State Effect: Correlation of Molecular Conformation, Crystal Packing and Colour in Perylene-3,4:9,10-Bis(Dicarboximide) Pigments. *Acta Crystallogr., Sect. B: Struct. Sci.* **1989**, *45*, 69−77.
(59) Liu, S.-G.; Sui, G.; Cormier, R. A.; Leblanc, R. M.; Gregg, B. A. Self-Organizing Liquid Crystal Perylene Diimide Thin Films: Spectroscopy, Crystallinity, and Molecular Orientation. *J. Phys. Chem. B* **2002**, *106*, 1307−1315.
(60) Jones, B. A.; Ahrens, M. J.; Yoon, M.-H.; Facchetti, A.; Marks, T. J.; Wasielewski, M. R. High-Mobility Air-Stable N-Type Semiconductors with Processing Versatility: Dicyanoperylene-3,4:9,10-Bis(Dicarboximides). *Angew. Chem., Int. Ed.* **2004**, *43*, 6363−6366.
(61) Kohn, P.; Ghazaryan, L.; Gupta, G.; Sommer, M.; Wicklein, A.; Thelakkat, M.; Thurn-Albrecht, T. Thermotropic Behavior, Packing, and Thin Film Structure of an Electron Accepting Side-Chain Polymer. *Macromolecules* **2012**, *45*, 5676−5683.
(62) Neese, F. The ORCA Program System. *WIREs Comput. Mol. Sci.* **2012**, *2*, 73−78.
(63) Maruani, J. *Molecules in Physics, Chemistry, and Biology: Molecular Phenomena in Biological Sciences*; Springer Netherlands: The Netherlands, 1989; Vol. *4*.
(64) Vydrov, O. A.; Voorhis, T. V. Nonlocal van der Waals Density Functional: The Simpler the Better. *J. Chem. Phys.* **2010**, *133*, No. 244103.
(65) Hujo, W.; Grimme, S. Performance of the van der Waals Density Functional VV10 and (Hybrid)GGA Variants for Thermochemistry and Noncovalent Interactions. *J. Chem. Theory Comput.* **2011**, *7*, 3866−3871.
(66) Krinichnyi, V. I. EPR Spectroscopy of Polarons in Conjugated Polymers and Their Nanocomposites. In *Polarons: Recent Progress and Perspectives*; Laref, A., Ed.; NOVA Science Publishers, Inc.: Hauppauge, NY, 2018; pp 1−105.
(67) Dyakonov, V.; Zoriniants, G.; Scharber, M.; Brabec, C. J.; Janssen, R. A. J.; Hummelen, J. C.; Sariciftci, N. S. Photoinduced Charge Carriers in Conjugated Polymer-Fullerene Composites Studied with Light-Induced Electron-Spin Resonance. *Phys. Rev. B* **1999**, *59*, 8019−8025.
(68) Baleg, A. A.; Masikini, M.; John, S. V.; Williams, A. R.; Jahed, N.; Baker, P.; Iwuoha, E. Conducting Polymers and Composites. In *Functional Polymers*; Mazumder, M. J.; Sheardown, H.; Al-Ahmed, A., Eds.; Springer: Cham, 2019; pp 1−54.
(69) Krinichnyi, V. I.; Yudanova, E. I.; Spitsina, N. G. Light-Induced EPR Study of Poly(3-Alkylthiophene)/Fullerene Composites. *J. Phys. Chem. C* **2010**, *114*, 16756−16766.
(70) Nelson, J. Diffusion-Limited Recombination in Polymer-Fullerene Blends and Its Influence on Photocurrent Collection. *Phys. Rev. B* **2003**, *67*, No. 155209.
(71) Molin, Y. N.; Salikhov, K. M.; Zamaraev, K. I. *Spin Exchange: Principles and Applications in Chemistry and Biology*; Springer-Verlag: Berlin, 1980.
(72) Houzé, E.; Nechtschein, M. ESR in Conducting Polymers: Oxygen-Induced Contribution to the Linewidth. *Phys. Rev. B* **1996**, *53*, 14309−14318.
(73) Krinichnyi, V. I.; Yudanova, E. I. Structural Effect of Electron Acceptor on Charge Transfer in Poly(3-Hexylthiophene)/Methanofullerene Bulk Heterojunctions. *Sol. Energy Mater. Sol. Cells* **2011**, *95*, 2302−2313.
(74) Zuppiroli, L.; Paschen, S.; Bussac, M. N. Role of the Dopant Counterions in the Transport and Magnetic-Properties of Disordered Conducting Polymers. *Synth. Met.* **1995**, *69*, 621−624.
(75) Nayeem, A.; Rananavare, S. B.; Sastry, V. S. S.; Freed, J. H. Heisenberg Spin Exchange and Molecular Diffusion in Liquid Crystals. *J. Chem. Phys.* **1989**, *91*, 6887−6905.
(76) Srinivasan, D.; Natarajan, T. S.; Rangarajan, G.; Bhat, S. V.; Wessling, B. Electron Spin Resonance Absorption in Organic Metal Polyaniline and Its Blend with PMMA. *Solid State Commun.* **1999**, *110*, 503−508.
(77) Huang, W. S.; MacDiarmid, A. G. Optical Properties of Polyaniline. *Polymer* **1993**, *34*, 1833−1845.
(78) Redfield, A. G. The Theory of Relaxation Processes. In *Advances in Magnetic and Optical Resonance*; Waugh, J. S., Ed.; Academic Press, 1965; Vol. *1*, pp 1−32.
(79) Benetis, N.-P.; Dmitriev, Y. Dynamical Effects in CW and Pulsed EPR. In *EPR of Free Radicals in Solids I: Trends in Methods and Applications*; Lund, A.; Shiotan, M., Eds.; Springer: Netherlands, 2013; Vol. *1*, pp 103−169.
(80) Carrington, F.; McLachlan, A. D., *Introduction to Magnetic Resonance with Application to Chemistry and Chemical Physics*; Harrer & Row, Publishers: New York, Evanston, London, 1967.
(81) Nechtschein, M. Electron Spin Dynamics. In *Handbook of Conducting Polymer*; Skotheim, T. A.; Elsenbaumer, R. L.; Reynolds, J. R., Eds.; Marcel Dekker: New York, 1997; pp 141−163.
(82) Pietronero, L. Ideal Conductivity of Carbon π-Polymers and Intercalation Compounds. *Synth. Met.* **1983**, *8*, 225−231.
(83) El Kadiri, M.; Parneix, J. P. Frequency- and Temperature-Dependent Complex Conductivity of Some Conducting Polymers. In *Electronic Properties of Polymers and Related Compounds*; Kuzmany, H.; Mehring, M.; Roth, S., Eds.; Springer-Verlag: Berlin, 1985; Vol. *63*, pp 183−186.
(84) Jayakrishnan, P.; Ramesan, M. T. Temperature Dependence of the Electrical Conductivity of Poly(Anthranilic Acid)/Magnetite Nanocomposites and the Applicability of Different Conductivity Models. *Polym. Compos.* **2018**, *39*, 2791−2800.

https://dx.doi.org/10.1021/acs.jpcc.0c02317
J. Phys. Chem. C 2020, 124, 10852−10869